

***In-silico* Studies of *Boerhavia diffusa* (Purnarnava) Phytoconstituents as ACE II Inhibitor: Strategies to Combat COVID-19 and Associated Diseases**

Rahul Maurya^{1,*}, Thirupataiah Boini¹, Lakshminarayana Misro¹, and Thulasi Radhakrishnan¹

¹National Ayurveda Research Institute for Panchakarma, Central Council for Research in Ayurvedic Sciences, Ministry of AYUSH, Government of India, Cheruthuruthy, Thrissur, Kerala 679531, India

Abstract – COVID-19 caused a catastrophe in human health. People infected with COVID-19 also suffer from various clinical illnesses during and after the infection. The *Boerhavia diffusa* plant is well known for its antihypertensive activity. ACE-II inhibitors and calcium channel blockers are reported as mechanisms for the antihypertensive activity of *B. diffusa* phytoconstituents. Various studies have said ACE-II is the virus's binding site to attack host cells. COVID-19 treatment commonly employs a variety of synthetic antiviral and steroidal drugs. As a result, other clinical illnesses, such as hypertension and hyperglycemia, emerge as serious complications. Safe and effective drug delivery is a prime objective of the drug development process. COVID-19 is treated with various herbal treatments; however, they are not widely used due to their low potency. Many herbal plants and formulations are used to treat COVID-19 infection, in which *B. diffusa* is the most widely used plant. The current study relies on discovering active phytoconstituents with ACE-II inhibitory activity in the *B. diffusa* plant. As a result, it can be used as a treatment option for patients with COVID-19 and related diseases. Different phytoconstituents of the *B. diffusa* plant were selected from the reported literature. The activity of phytoconstituents against ACE-II proteins has been studied. Molecular docking and ligand-protein interaction computation tools are used in the *in-silico* experiment. Physicochemical, drug-likeness, water solubility, lipophilicity, and pharmacokinetic parameters are used to evaluate phytoconstituents. Liriodenine has the best drug-likeness, bioactivity, and binding score characteristics among the selected ligands. The *in-silico* study aims to find the therapeutic potential of *B. diffusa* phytoconstituents against ACE-II. Targeting ACE-II also shows an effect against SARS-CoV-2. It can serve as a rationale for designing a drug for patient infected with COVID-19 and associated diseases.

Keywords – ACE-II protein, COVID-19, *Boerhavia diffusa*, *In-silico* molecular docking, ligands-receptor interaction

Introduction

The COVID-19 pandemic is a viral disease. The causative organism of this disease is the SARS-CoV-2 virus (severe acute respiratory syndrome coronavirus 2). The impaired immune system is the prime factor behind the pathogenesis of COVID-19. The virus has a spherical shape with a diameter of approximately 60 – 140 nm.¹ It is a single-stranded RNA virus consisting of a spike, membrane, envelope nucleocapsid, and glycoprotein. The nucleoside protein is associated with the genomic RNA, while other proteins construct protein envelopes around it. Viral infection involves cell penetration and used host cell mechanisms to make replicas of the virus and then release

it from the host cell. S1 and S2 subunits of spike protein plays a significant role in regulating virus entry into host cells. The receptor-binding site (RBS) is present in the S1 subunit. It binds with the peptide site (PS) of the angiotensin-converting enzyme-II (ACE-II) protein.² The S2 subunit facilitates membrane fusion and entangles the spike protein to the virion membrane.³ It is a crucial step that promotes the fusion of the host cell membranes and virus. The spike protein of SARS-CoV-2 acts as a substrate for ACE-II receptors. The virus could infect the cells expressing ACE-II receptors, including alveolar, neuroepithelial, endothelial, renal, macrophages, monocytes, neurons, glial, and intestinal epithelial cells.⁴ As a result, genetic changes in the ACE-II sequence may alter the molecular interaction of the RBS and PS, which influence both the severity of the disease and host susceptibility to the virus. ACE-II is present on chromosome Xp22 and occupies 39.98 kb of genomic DNA. It has 20

*Author for correspondence

Rahul Maurya, National Ayurveda Research Institute for Panchakarma, cheruthuruthy, Thrissur, Kerala, 679531, India.
Tel: +91-04884-262543; E-mail: mauryabrahul@gmail.com

introns and 18 exons. It is a type-I membrane-bound glycoprotein with an 805 amino acid catalytic domain.⁵ Loop ridges, helices, and some beta sheets cover the ACE-II protein. ACE-II has two domains: a carboxyl-terminal domain that aids receptor binding and an amino-terminal domain with one zinc metallopeptidase active site. Angiotensin (Ang) is converted into Ang I by renin, whereas Ang I is converted into Ang II by ACE-II. Ang II is responsible for vasoconstriction, hypertension, and cardiac hypertrophy.⁶ Due to the widespread expression of ACE-II receptors in several organs, which may cause hypertension, diabetes, and cancer are the main risk factors for the progression and prognosis of COVID-19.⁷⁻⁹ Furthermore, the COVID-19 clinical history reveals gender differences in morbidity and mortality. Males are nearly three times more likely to be infected than females.¹⁰ Numerous research trials have been performed using synthetic drug molecules as antivirals or immunomodulators.¹¹ Although some drugs have been prescribed for COVID-19 patients, these synthetic compounds have a toxic effect that could cause overstimulation and a decline in cellular functions.¹² For instance, 2-DG (2-deoxy-D-Glucose) and hydroxy-chloroquinone have lately been utilized to decrease COVID-19 infection.¹³ However, it has been noted that they may cause increased melanin, skin rashes, ophthalmic, disorientation, and cardiac damage. Therefore, there is an urgent need to replace synthetic compounds with other phytoconstituents that offer therapeutic support to COVID-19 patients and collaborate to enhance organism health. The phytochemicals extracted from *Boerhavia diffusa* are classified as alkaloids, rotenoids, phenolics, glycosides, nucleosides, lignans, and steroids.^{14,15} The root of *B. diffusa* plant consisting of lignin, lirioidendrin (syringaresinol β -D-diglycoside or acanthoside D). It has anti-inflammatory and cardioprotective activity. Lirioidendron mitigated sciatic endometriosis-related pain in rats by suppressing the inflammation and regulating the PI3K/Akt/mTOR signaling pathway.¹⁶ In the case of acute lung injury, oral administration of lirioidendron causes a significant reduction of pulmonary inflammation in LPS-induced mice.¹⁷ Boeravinone B diminished myocardial infarction by lowering oxidative stress in the cardiac tissue by decreasing expressions of caspase-3 & 9, p53, BAX, cyt C, NGAL, TNF, IL-1 & 6, and increasing Bcl-2 expression.¹⁸ Eupalitin has anti-neuroinflammation in *in-vitro* microglial cell lines.¹⁹ Several active phytoconstituents of the *B. diffusa* plant, including lirioidendron, boeravinone J, boerhavisterol, bioquercetin, 2-3-4 beta-ecdysone, kaempferol, biorobin, quercetin, and *trans*-caftaric acid, inhibited SAR-CoV-2

Main Protease.²⁰ To save money and time, researchers are conducting *in-silico* methods. The primary object of ongoing pharmaceutical research is the target and lead discovery prediction. To properly understand the pharmacological activity of bioactive compounds, *in-silico* approaches are combined with other advanced scientific tools to support innovation in health services, academic and industrial research, and development. The *in-silico* study suggests that phytoconstituents from *B. diffusa* plants have therapeutic potential in attenuating ACE-II expression. Using phytoconstituents to target ACE-II against SARS-CoV2 could be a rational approach for developing future drugs for COVID and other related diseases.

Experimental

Preparation of ligands – The *in-silico* studies is crucial in identifying ligands against the target. To be a drug, phytoconstituents must obey Lipinski's rule of five (Supplementary data Table 1). Phytoconstituents of *B. diffusa* were downloaded in SDF format from the Indian medicinal plants, phytochemistry, and therapeutics (IMPPAT 2.0)²¹ database, and some phytocompounds were drawn using ChemDraw. All the 3D structures are saved in SDF format. The drug-likeness, physicochemical, lipophilicity, solubility, and pharmacokinetic properties of different phytoconstituents were studied by SwissADME.²² The energy minimization can be done using the UFF algorithm in PyRx software. 2-deoxy-D-Glucose (2-DG) is used as a controlled drug.

Preparation of protein – The 3D structure of the ACE-II protein (code 1R4L) was downloaded from the protein data bank (<http://www.rcsb.org>) in PDB format.²³ The X-ray diffraction of target proteins is used to select them for docking studies. The chosen protein should not have any protein breaks in its whole 3D shape.²⁴ The R-value around 0.2 showed that the selected protein model is efficient for molecular docking studies. The selected protein structure was associated with the ligand (2-acetamido-2-deoxy- β -D-glucopyranose). It was prepared by using Biovia discovery studio software. The ligand and water molecule were removed from the protein, and polar hydrogen was added to the protein and saved in PDB format for docking analysis.

***In-silico* molecular docking study** – *In-silico* molecular docking predicts the binding affinity of the receptor protein and ligand. The prepared ligands and protein receptor were selected for molecular docking. PyRx software was used to conduct the *in-silico* docking study. Protein and ligands are saved in PDBQT format after

being identified as macromolecules and ligands. The UFF force field was chosen to minimize ligand energy. The PyRx software's vina wizard tool docks each ligand with the appropriate protein. For docking of ligands X, Y, and Z, a grid box dimension was set to 60. The best interaction was chosen based on the lowest binding energy (Kcal/mol). The lowest binding energy model was chosen and saved as a PDB file. The discovery studio displays the minimum binding energy output model. The protein-ligand interaction, types of amino acids involved, and types of bonds formed between amino acid residue and ligands were analyzed and saved for further study.

In-silico ADME analysis – The SwissADME (<http://www.swissadme.ch>) is an available access web tool for Pharmacokinetic ADME ligands studies. This tool provides various physicochemical, pharmacokinetics, lipophilicity, drug-likeness, and water solubility parameters. Lipinski's rule of five gives information on the drug-likeness of orally active compounds. The boiled egg illustration demonstrated whether the ligand could cross the blood-brain barrier and enter the gastrointestinal membrane. The screened phytoconstituents' absorption, distribution, metabolism, and excretion characteristics were investigated. This study's findings were helpful in the selection of active phytoconstituents.

Analysis of specific cellular pathway – The cellular pathway utilized by coronavirus is obtained from open access source KEGG (<https://www.genome.jp/kegg/pathway.html>). The pathway involved with the ACE-II receptor and coronavirus spike protein substrate was described in Fig. S1.

Receptor-substrate interaction by STRING network analysis – STRING (Search tool for Retrieval of Interacting Genes) is an online database to predict receptor-substrate interaction and describe their functional activity. The database provides information about a substrate's biological processes, cellular components, and molecular actions.

Bioactivity score analysis using Molinspiration tool – Molinspiration (<http://www.molinspiration.com/cgi-bin/properties>) identifies the drug resemblance characteristics of the substance based on different descriptors. Molinspiration tools describe the bioactive score of phytoconstituents against the receptors like protease, GPCR, ion channel, kinase, and proteins. A receptor-substrate complex dynamic behavior finds out by the bioactive score. A bioactive score greater than 0 considers a good score for complexes.

Results and Discussion

The experimental work is based on the execution of an *in-silico* molecular docking study to predict the protein-ligand interaction. The binding of phytoconstituents with ACE-II receptors causes the down-regulation of ACE activity. Docking algorithms enforced the phytoconstituents' stimulating and inhibiting properties with ACE-II receptors, establishing a link between ligand structure and activity.

In the proposed work, more than 50 phytoconstituents were selected from the *B. diffusa* plant through the IMPPAT database, and some phytoconstituents were drawn using the ChemDraw tool. ACE-II receptor was docked with all the phytoconstituents. The docking interaction and energy minimization scores are given in Table 2. However, β -carotene, repenol, liriodenine, and diffusaroteniod were observed to be the most efficient. The observed binding energy of β -carotene, repenol, liriodenine, and diffusaroteniod with ACE-II receptor is -10.7 , -10.3 , -10.1 , and -10.1 Kcal/mol, respectively. 2-DG was selected as a control for the target ACE-II receptor. 2-DG is the most commonly used synthetic drug against COVID infection. The binding energy of 2-DG against the ACE-II receptor is -5.7 Kcal/mol. The interaction of 2-DG, β -carotene, repenol, liriodenine, and diffusarotenoid is depicted in Fig. 1. The interaction of different amino acid residues of 1R4L with ligands (β -carotene, repenol, liriodenine, and diffusarotenoid, and 2-DG) is given in Table 2. β -carotene interacts with the Van der Waal and Pi-Alkyl bond. Liriodenine interact with Van der Waal, H-bond, Pi-Pi stacked, T-shaped and Pi-alkyl bond. The H-bond observed between the oxygen and nitrogen atom of liriodenine with ARG 518. Liriodendrin interacts with the Van der Waal, H-bond, C-H bond, Pi-Pi T-shaped, alkyl, and Pi-Alkyl. The H-bond observed between the pyranose OH group of Liriodendrin and heteroatom of LYS 562 and GLN 98 amino acids. The Oxygen atom of the bicyclic five-member ring of the liriodenine forms an H bond with LYS 562 and ASP 206 amino acids. Repenol ligand interact with amino acid residue by Van der Waal, H-bond, Pi-Pi stacked, and Pi-anion. The oxygen atom of the carbonyl group and phenolic OH of repenol formed H-bond with ARG 518 and ASP 367 amino acids, respectively. Diffusarotenoid interacts with amino acid residue by Van der Waal, H-bond, C-H bond, Pi-cation & anion, alkyl & Pi-alkyl. The oxygen atom of the carbonyl group and phenolic OH of diffusarotenoid formed H-bond with ARG 518 and PRO 346 amino acids, respectively. The control ligand 2-DG interacts with protein by

Table 1. Physicochemical, kinetic, and drug likeness characters of phytoconstituents

Parameters	Beta carotene	Liriodenine	Repenol	Diffusarotenoid	2-DG
Formula	C40H56	C17H9NO3	C18H12O10	C22H20O7	C6H12O5
Binding Score	-10.7	-10.1	-10.3	-10.1	-5.7
Molecular weight	536.87 g/mol	275.26 g/mol	388.28 g/mol	396.39 g/mol	165.15 g/mol
Num. heavy atoms	40	21	28	29	11
Num. aromatic heavy atoms	0	16	16	16	0
Fraction Csp3	0.45	0.06	0.11	0.27	1.00
Num. rotatable bonds	10	0	3	5	1
Num. H-bond acceptors	0	4	10	7	5
Num. H-bond donors	0	0	4	2	4
Molar Refractivity	184.43	76.67	92.92	106.79	34.57
TPSA	0.00 Å ²	48.42 Å ²	155.89 Å ²	106.20 Å ²	90.15 Å ²
Lipophilicity Log <i>P</i> _{o/w} (iLOGP)	7.79	2.14	2.20	3.48	0.58
Log <i>P</i> _{o/w} (XLOGP3)	13.54	3.39	2.29	3.78	-1.96
Water Solubility Log ESOL	-11.04	-4.25	-3.91	-4.76	0.44
Drug likeness Lipinski	No; 2 violations: MW>500, MLOGP>4.15	Yes; 0 violation	Yes; 0 violation	Yes; 0 violation	Yes; 0 violation
Bioavailability Score	0.17	0.55	0.55	0.55	0.55
Synthetic accessibility	6.19	2.77	4.09	4.36	3.90
GI absorption	Low	High	Low	High	High
BBB permeant	No	Yes	No	No	No
P-gp substrate	Yes	Yes	No	No	No
CYP1A2 inhibitor	No	Yes	No	Yes	No
CYP2C19 inhibitor	No	No	No	No	No
CYP2C9 inhibitor	No	No	Yes	Yes	No
CYP2D6 inhibitor	No	No	No	No	No
CYP3A4 inhibitor	No	Yes	No	Yes	No
Log <i>K</i> _p (skin permeation)	0.04 cm/s	-5.57 cm/s	-7.04 cm/s	-6.03 cm/s	-8.70 cm/s

Table 2. Binding interaction between ligands and protein 1R4L

Ligand molecule	Binding energy (Kcal/mol)	Amino acid interaction with ligand
Beta carotene	-10.7	Vander waal (18): ASP 269 & 350, TRP 271 & 349, ARG 273, 393, & 514, TYR 515 & 385, ALA 348, PRO 346, THR 371 & 347, GLU 375, PHE 504, HIS 378 & 374, ASN 394. Pi-Alkyl (6): PHE 274, HIS 345 & 505, TYR 510, PHE 390 & 40. Vander waal (5): ASP 367, THR 276 & 445, GLU 375 & 406
Liriodenine	-10.1	H-bond (1): ARG 518 Pi donar H bond (1): THR 371 Pi-Pi stacked & T-shaped (3): PHE 274, HIS 345 & 374. Vander waal (12): GLU 398 & 564, SER 511 & 563, TRP 203 & 199, TYR 510, ASP 509, LYS 187, GLY 205 & 211, ARG 514. H-bond (3): GLN 98, LYS 560, ASP 206.
Liriodendrin	-8.5	C-H bond (8): PRO 565, LEU 95, VAL 209, LYS 562, GLN 98, GLU 208, TYR 202, ASP 206. Pi-Pi T-shaped (1): TYR 202. Alkyl & Pi-Alkyl (2): LEU 95 & 395. Unfavorable donor-donor (1): ASN 210. Vander waal (15): ARG 203, HIS 374, 378 & 505, TYR 515, GLU 402, ZN 803, PHE 504, THR 347, HIS 345, PRO 346, ASP 368, MET 360, THR 276 & 445.
Repenol	-10.3	H-bond (2): APG 518, ASP 367. Pi-Pi stacked (1): PHE 274. Pi-Anion (1): GLU 375. Unfavorable acceptor-acceptor (1): THR 371. Vander waal (12): GLU 145, CYS 344 & 361, ASP 368 & 378, MET 360, THR 276, 347, 371 & 445, GLU 402, HIS 345.
Diffusarotenoid	-10.1	H-bond: PRO 346, ARG 518. C-H Bond (5): PRO 346, HIS 345, THR 371, ASP 367, PHE 274. Pi-Cation & Anion (2): GLU 375, ARG 273. Alkyl & Pi-Alkyl (4): LYS 363, HIS 374 & 378, TYR 515. Vander waal (10): ARG 273, 514 & 518, HIS 345, 374 & 378, GLU 372, 402 & 406, PHE 504.
2-Deoxy-D Glucose	-5.7	H-bond (2): TYR 515, HIS 505. C-H bond (1): HIS 505.

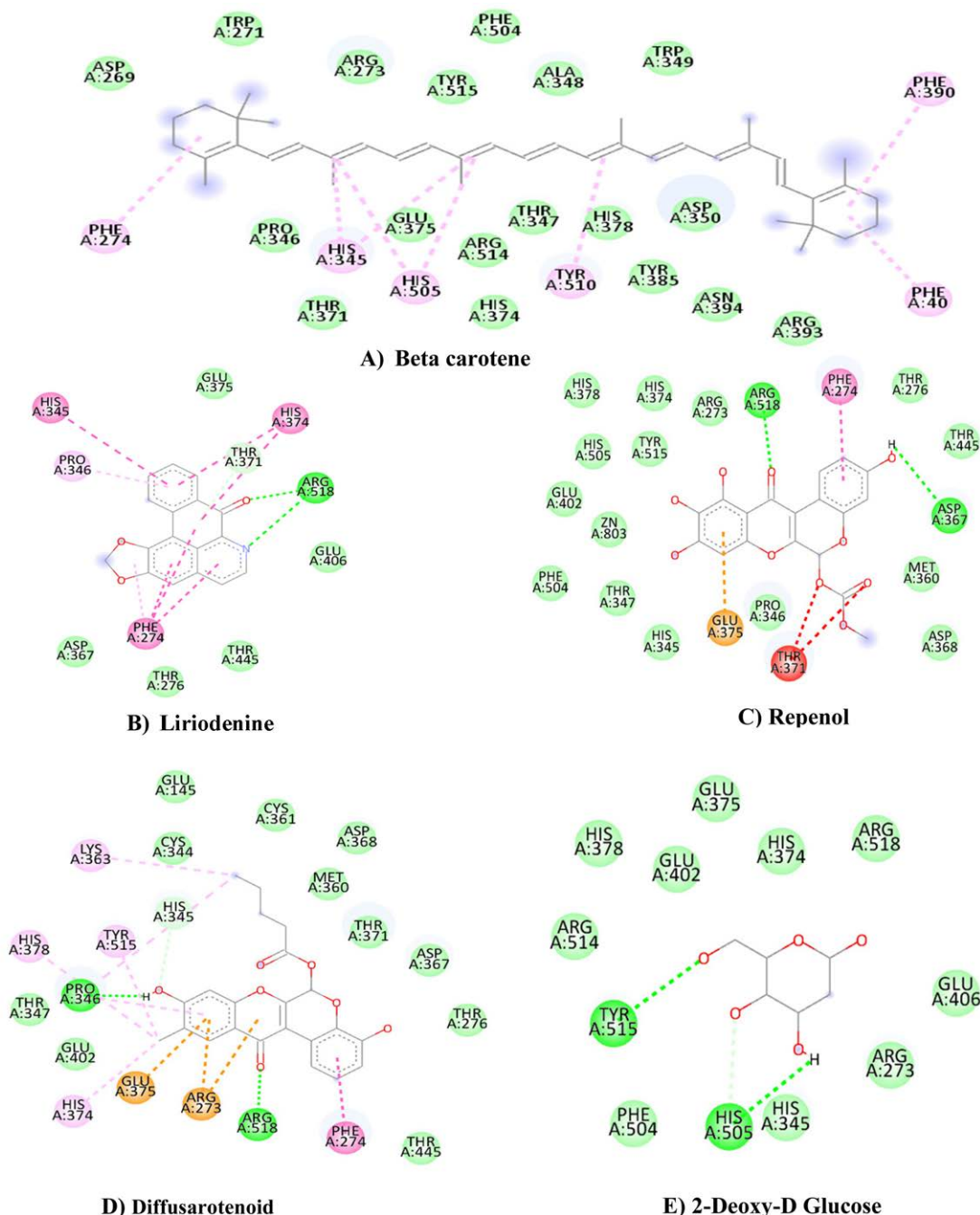


Fig. 1. *In-silico* molecular docking study of selective phytoconstituents of *B. diffusa* plant with ACE-II protein (code 1R4L).

forming H-bond, Van der Waal, and C-H bond. The OH of 2-DG formed H-bond with TYR 515 and HIS 505 amino acids, respectively. The amino acid residue of 1R4L protein given in Table 2 interacts with 2-DG. Although similar amino acid residue interaction found in *B. diffusa* plant extract (β -carotene: ARG 273, 514, PHE 504, HIS 374 & 378; Repenol: HIS 374 & 388, GLU 402, PHE 504; diffusarotenoid: ASP 378, GLU 402, HIS

345; liriodenine: ARG 514). It exhibited that this plant extract may have antiviral properties.

The binding affinity of phytoconstituents with ACE-II is given in Table S1. Around 40 phytoconstituents of the *B. diffusa* plant have greater and ten phytoconstituents have a lesser affinity than control ligand 2-DG. Some of the phytoconstituents that have a higher affinity as compared to control ligand 2-DG are β -carotene -10.7 ,

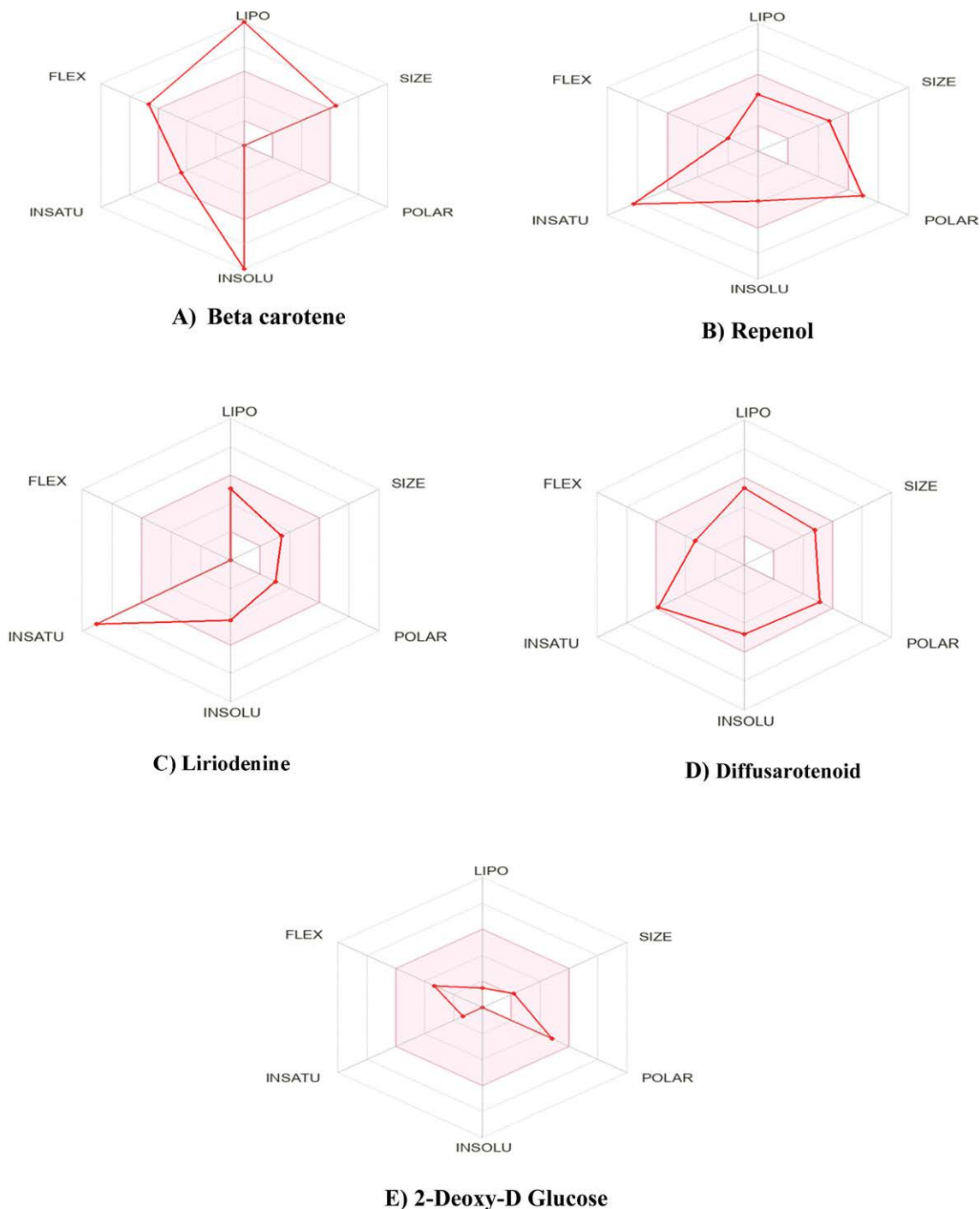


Fig. 2. Physiochemical property of selective phytoconstituents of *B. diffusa* plant and 2-deoxy-D-glucose.

repenol -10.3 , liriodenine -10.1 , diffusarotenoid -10.1 , boeravinone B -10 , boeravinone F -10 , stigma sterol glucoside -10 , b-amyrin -10 , campesterol glucoside -10 , boeravinone A -9.8 , stigmas-5 -9.8 ; It reveals that *B. diffusa* plant extract has ACE-II inhibitor properties.

The proposed molecular docking studies suggested the characteristics of greater binding affinity of selected

phytoconstituents with ACE-II compared to the synthetic inhibitors 2-DG; it shows the therapeutic relevance of the *B. diffusa* plant in combating COVID-19-associated problems.

A SwissADME analysis was carried out to identify the drug-likeness characteristics of screened phytoconstituents. Lipinski et al. proposed various parameters to

find the drug-likeness character of orally administered drugs. The colored zone of the radar is the suitable physiochemical area for oral bioavailability. The desired value of the parameters like; molecular weight not more than 500 g/mol, lipophilicity (XLOGP3) should be less than 5, polarity in the range of 20–130 Å, no. of rotatable bonds should be less than 9, and the value of water solubility parameter Log S(ESOL) in the range –6 to 0;²⁵ defining the physiochemical parameters of β -carotene, repenol, liriodenine, and diffusarotenoid showed significant response with control 2-DG (Fig. 2).

Liriodenine, repenol, and diffusarotenoid obey all the Lipinski rules of five, like control 2-DG molecules. It exhibited that it can be orally administered and absorbed by GIT²⁶. In addition, liriodenine, repenol, and diffusarotenoid have 0 violations of Lipinski and an almost similar bioavailability score of 0.55 as 2-DG. The phytoconstituents given in Table 1 had a feature to be drug molecules; however, a molecule having a greater affinity than 2-DG is found to be the better option for drug discovery. The bioavailability and absorption of the selected candidate can be improved in the future by formulation developments.

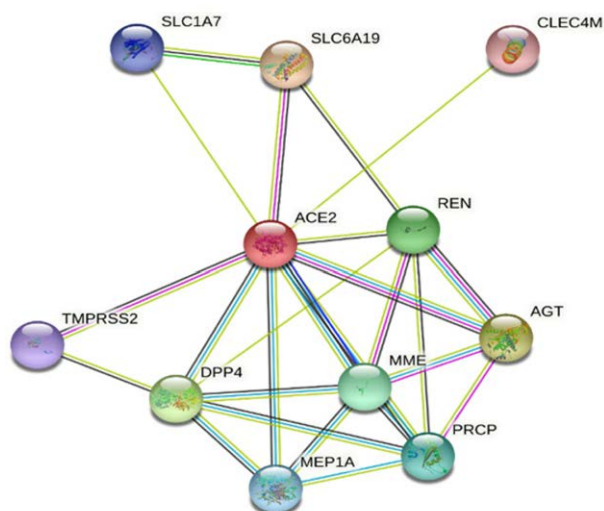


Fig. 3. Network formation of ACE2 STRING

Fig. 3 exhibited the interaction of ACE-II receptors with endogenous molecules detected by the STRING target network (string-db.org). ACE-II interacts with various protein given in Fig. 3. Dipeptidyl peptidase 4 (DPP4) is a cell surface glycoprotein receptor involved in T-cell activation. Lysosomal pro-X carboxypeptidase (PRCP) inactivates angiotensin and bradykinin. Transmembrane protease serine 2 (TMPSR S2) is a serine protease that promotes coronavirus uptake. C-type lectin domain family 4 members (CLEC 4 M) mediate the pathogen's endocytosis. Renin (REN) is an endopeptidase that produces angiotensin I from angiotensinogen. Angiotensinogen (AGT) regulates blood pressure, electrolyte homeostasis, and body fluid through the renin-angiotensin system (RAS).

The physiochemical parameters in Table 1 represent selected phytoconstituents showing drug-likeness characters similar to the 2-DG. The lipophilicity parameters of phytoconstituents presented in Table 1 exhibit positive values, which indicates a higher lipid affinity than 2-DG. The order of lipophilicity of the selected compounds is β -carotene > diffusarotenoid > repenol > liriodenine > 2-DG.

KEGG analysis was performed to predict the clinical significance of the identified target and the involvement of ACE-II. Around ten targets, including those in Fig. 3, were identified via string analysis²⁷. These targets were mainly associated with the clinical activity of ACE-II. The KEGG cell signaling pathways related to COVID-19 and the renin-angiotensin system are shown in Fig. S1. Furthermore, the viral spike protein was received by ACE-II and NRP1 in the COVID-19 pathway and transferred into the cell via endocytosis or membrane fusion. Ang I and II enter the host cell via MAS1 and AT1R, followed by ADAM17, TNFR, EGFR, and TLR2/4.

Further, we identified the bioactivity scores to determine the potency of phytoconstituents (Table 3). The result reveals that liriodenine has a more excellent enzyme inhibitor score than the control drug, 2-DG. Bioactivity scores of phytoconstituents and the control drug 2-DG were compared, indicating that the proposed phytocons-

Table 3. Bioactivity scores of selected phytoconstituents

Bioactivity	Beta carotene	Repenol	Liriodenine	Diffusarotenoid	2 DG
GPCR ligand	-0.04	-0.20	0.00	-0.30	-0.62
Ion channel modulator	-0.15	-0.35	-0.08	-0.52	0.07
Kinase inhibitor	-0.15	-0.11	0.44	-0.33	-1.00
Nuclear receptor ligand	0.40	0.08	-0.10	0.26	-0.76
Protease inhibitor	-0.06	-0.41	-0.23	-0.37	-0.17
Enzyme inhibitor	0.17	0.05	0.51	-0.14	0.31

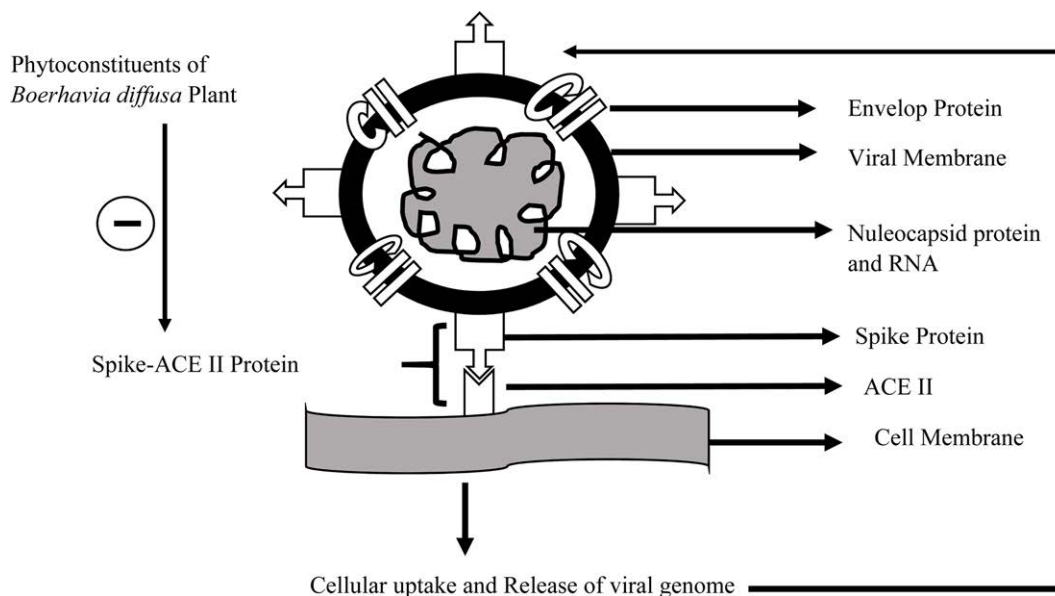


Fig. 4. ACE II inhibitors mechanism of *B. diffusa* plant phytoconstituents to combat COVID-19.

tituents might be used as an alternative to the treatment of COVID-19.

Identifying selective targets leads to determining mechanistic pathways involved in coronavirus integration into the biological system and related chronic diseases. Coronavirus entry into the human genome is aided by ACE-II.²⁸ The phytoconstituents of *B. diffusa* have shown explicit findings against coronavirus. Molecular docking of the phytoconstituents with protein has provided good binding affinity, and the study is presented to assess ligands *in-vitro* as well as *in-vivo* study.

Out of all phytoconstituents, liriodenine has exhibited good affinity, obeys Lipinski's drug-likeness, and has a more enzyme inhibitor score. Downstream to molecular mechanism, ACE-II protein is also associated with other cellular mechanisms like cell growth, vasodilation, and amyloid- β metabolic activities²⁹. We propose phytoconstituents of the *B. diffusa* plant as ACE-II inhibitors to combat COVID-19 (Fig. 4). However, such findings need further confirmation by utilizing *in-vitro* experiments and molecular dynamics simulation.

In conclusion, herbal or medicine plants have the potential to treat clinical illnesses. The proposed study investigated the clinical effectiveness of some phytoconstituents extracted from the *B. diffusa* plant. The findings are expected to pique the scientific community's interest in drug development against COVID-19, for which no specific drug has been discovered using herbal products. The forecast prospect of the proposed study is to explore the antiviral activity of selected phytoconstituents-rich

plant extract by performing *in-vitro* cell line study. The safety and efficacy will ensure by *in-vivo* studies. The approach of the study is to investigate herbal bioactive compounds for COVID-19 and associated diseases moreover, similar research can be done with other medicinal plants. Furthermore, our research is being expanded to look at the effects of other diseases that may be contributing to the progression of the coronavirus.

Acknowledgments

This work was supported by a grant (3-66/2021-CCRAS/Admn/IMR/1631) from the Central Council for Research in Ayurvedic Sciences, Ministry of AYUSH, Government of India. The authors also thankful to DG, CCRAS and Director, National Ayurveda Research Institute for Panchakarma, Thrissur, India for providing continuous support and encouragement.

Conflicts of Interest

The authors declare that they have no conflicts of interest.

References

- (1) Porter, J.; Blau, E.; Gharagozloo, F.; Martino, M.; Cerfolio, R.; Duvvuri, U.; Caceres, A.; Badani, K.; Bhayani, S.; Collins, J.; Coelho, R.; Rocco, B.; Wiklund, P.; Nathan, S.; Parra-Davila, E.; Ortiz-Ortiz, C.; Maes, K.; Dasgupta, P.; Patel, V. *BJU Int.* **2020**, *126*, 225–234.
- (2) Hashemi, S. M. A.; Thijssen, M.; Hosseini, S. Y.; Tabarraei, A.;

- Pourkarim, M. R.; Sarvari, J. *Arch. Virol.* **2021**, *166*, 2089–2108.
- (3) Jackson, C. B.; Farzan, M.; Chen, B.; Choe, H. *Nat. Rev. Mol. Cell Bio.* **2022**, *23*, 3–20.
- (4) Gu, W.; Gan, H.; Ma, Y.; Xu, L.; Cheng, Z. J.; Li, B.; Zhang, X.; Jiang, W.; Sun, J.; Sun, B.; Hao, C. *Virol. J.* **2022**, *19*, 49.
- (5) Singh, H.; Choudhari, R.; Nema, V.; Khan, A. A. *Microb. Pathog.* **2021**, *150*, 104621.
- (6) Bhushan, S.; Xiao, Z.; Gao, K.; Mao, L.; Chen, J.; Ping, W.; Hong, W.; Zhang, Z. *Curr. Probl. Cardiol.* **2022**, *48*, 101162.
- (7) Cheng, H.; Wang, Y.; Wang, G. Q. *J. Med. Virol.* **2020**, *92*, 726–730.
- (8) Bhowmick, N. A.; Oft, J.; Dorff, T.; Pal, S.; Agarwal, N.; Figlin, R. A.; Posadas, E. M.; Freedland, S.; Gong, J. *Endocr. Relat. Cancer* **2020**, *27*, R281–R292.
- (9) Zaki, N.; Alashwal, H.; Ibrahim, S. *Diabetes Metab. Syndr.* **2020**, *14*, 1133–1142.
- (10) Peckham, H.; de Gruijter, N. M.; Raine, C.; Radziszewska, A.; Ciurtin, C.; Wedderburn, L. R.; Rosser, E. C.; Webb, K.; Deakin, C. T. *Nat. Commun.* **2020**, *11*, 6317.
- (11) Nugraha, R. V.; Ridwansyah, H.; Ghozali, M.; Khairani, A. F.; Atik, N. *Evid. Based Complement. Alternat. Med.* **2020**, *2020*, 2560645.
- (12) Creagh, S.; Warden, D.; Latif, M. A.; Paydar, A. *Clin. Radiol. Imaging. J.* **2018**, *2*, 000116.
- (13) Huang, Z.; Chavda, V. P.; Vora, L. K.; Gajjar, N.; Apostolopoulos, V.; Shah, N.; Chen, Z. S. *Front. Pharmacol.* **2022**, *13*, 899633.
- (14) Gaur, P. K.; Rastogi, S.; Lata, K. *Phytomed. Plus* **2022**, *2*, 100260.
- (15) Maurya, R.; Boini, T.; Misro, L.; Thulasi, R.; Singh, R. *Curr. Hypertens. Rev.* **2023**, *19*, 1–17.
- (16) Gong, J.; Xue, L.; Wei, M.; Han, W.; Jing, S. *Arch. Med. Sci.* **2021**, *in press*.
- (17) Yang, L.; Li, D.; Zhuo, Y.; Zhang, S.; Wang, X.; Gao, H. *Inflammation* **2016**, *39*, 1805–1813.
- (18) Chen, Y.; Peng, L.; Shi, S.; Guo, G.; Wen, H. *J. Cell. Mol. Med.* **2021**, *25*, 6403–6416.
- (19) Kumar, J. R.; Varadaraju, K. R. *Eur. J. Mol. Clin. Med.* **2021**, *8*, 2207–2216.
- (20) Rutwick Surya, U.; Praveen, N. *Virusdisease.* **2021**, *32*, 46–54.
- (21) Vivek-Ananth, R. P.; Mohanraj, K.; Sahoo, A. K.; Samal, A. *bioRxiv* **2022**, 496609.
- (22) Daina, A.; Michielin, O.; Zoete, V. *Sci. Rep.* **2017**, *7*, 42717.
- (23) Towler, P.; Staker, B.; Prasad, S. G.; Menon, S.; Tang, J.; Parsons, T.; Ryan, D.; Fisher, M.; Williams, D.; Dales, N. A.; Patane, M. A.; Pantoliano, M. W. *J. Biol. Chem.* **2004**, *279*, 17996–18007.
- (24) Upreti, S.; Prusty, J. S.; Pandey, S. C.; Kumar, A.; Samant, M. *Mol. Divers.* **2021**, *25*, 1795–1809.
- (25) Lawal, B.; Liu, Y. L.; Mokgautsi, N.; Khedkar, H.; Sumitra, M. R.; Wu, A. T. H.; Huang, H. S. *Biomedicines* **2021**, *9*, 92.
- (26) Andrews, C. W.; Bennett, L.; Yu, L. X. *Pharm. Res.* **2000**, *17*, 639–644.
- (27) Wicik, Z.; Eyileten, C.; Jakubik, D.; Simões, S. N.; Martins Jr, D. C.; Pavão, R.; Siller-Matula, J. M.; Postula, M. *J. Clin. Med.* **2020**, *9*, 3743.
- (28) Luo, J.; Lu, S.; Yu, M.; Zhu, L.; Zhu, C.; Li, C.; Fang, J.; Zhu, X.; Wang, X. *Gene* **2021**, *768*, 145325.
- (29) Rezaei, M.; Ziai, S. A.; Fakhri, S.; Pouriran, R. *J. Cell. Physiol.* **2021**, *236*, 2430–2442.

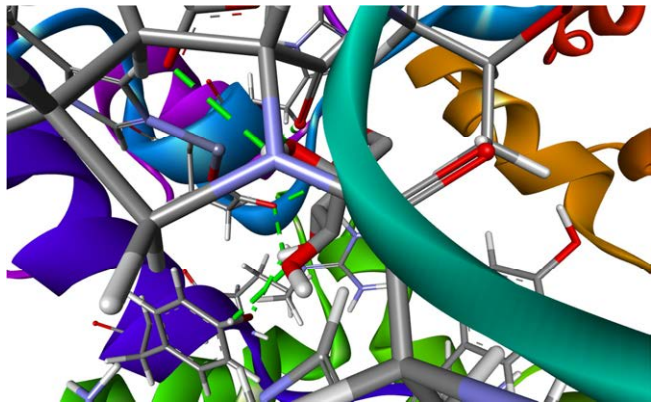
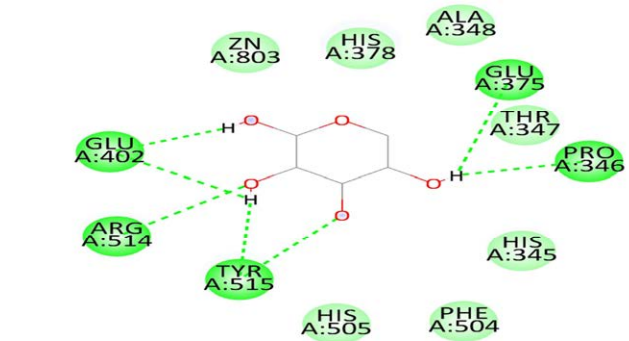
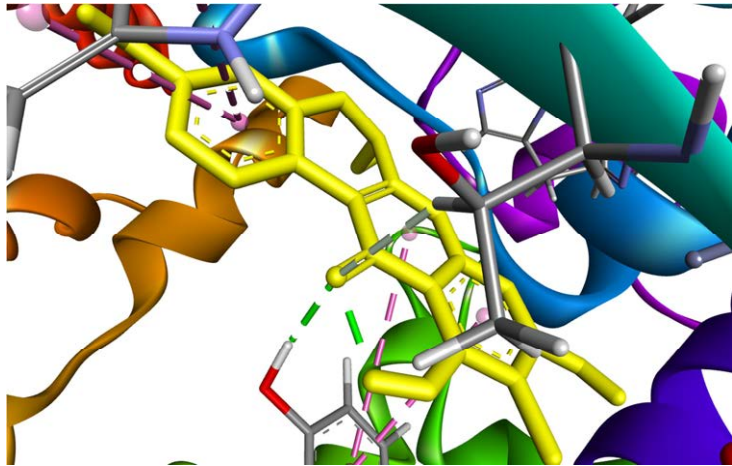
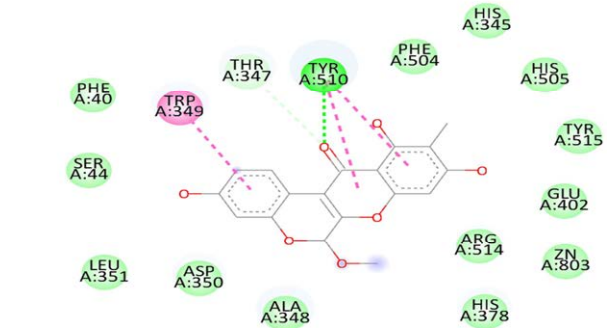
Received February 2, 2023

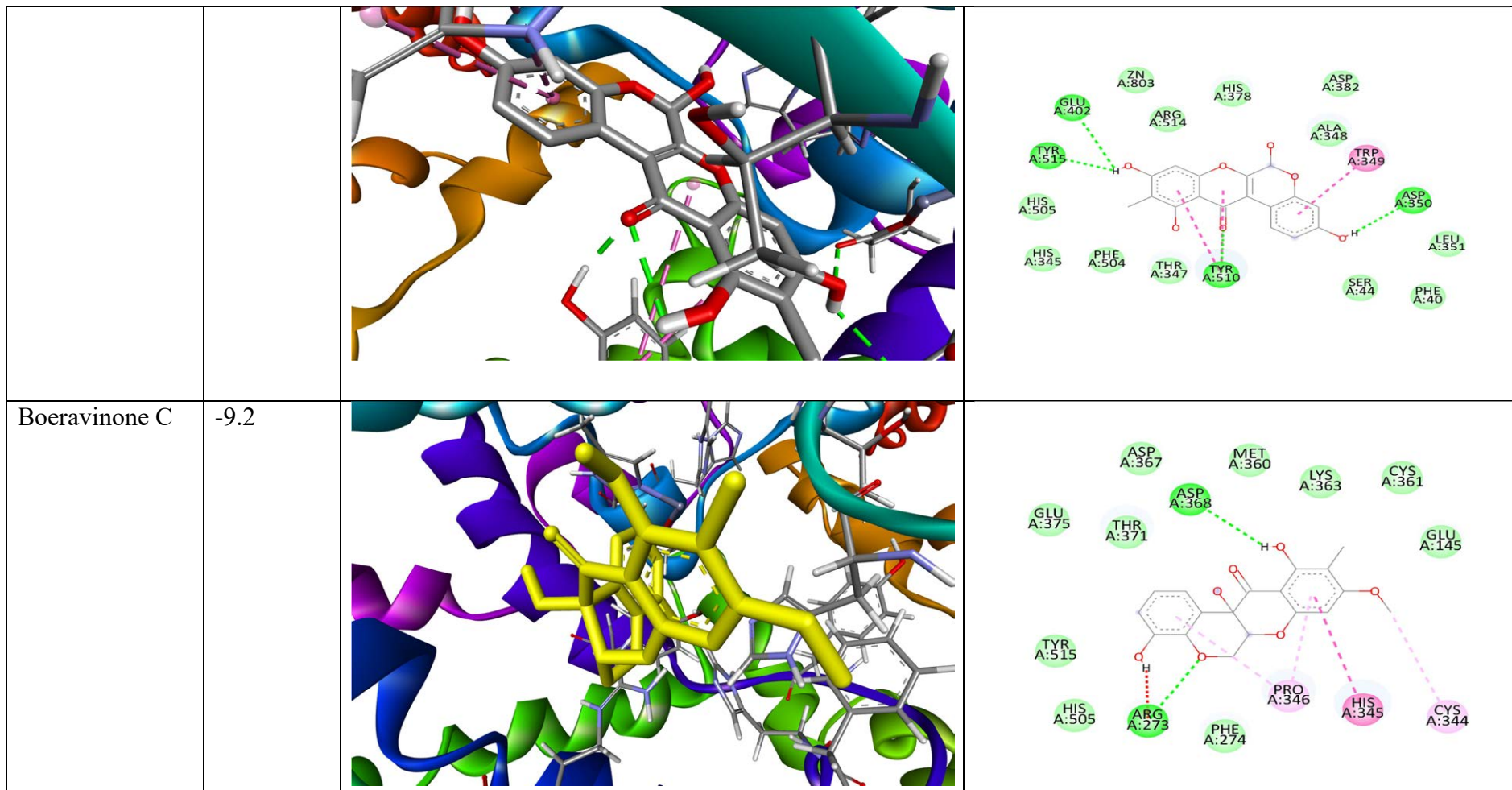
Revised June 12, 2023

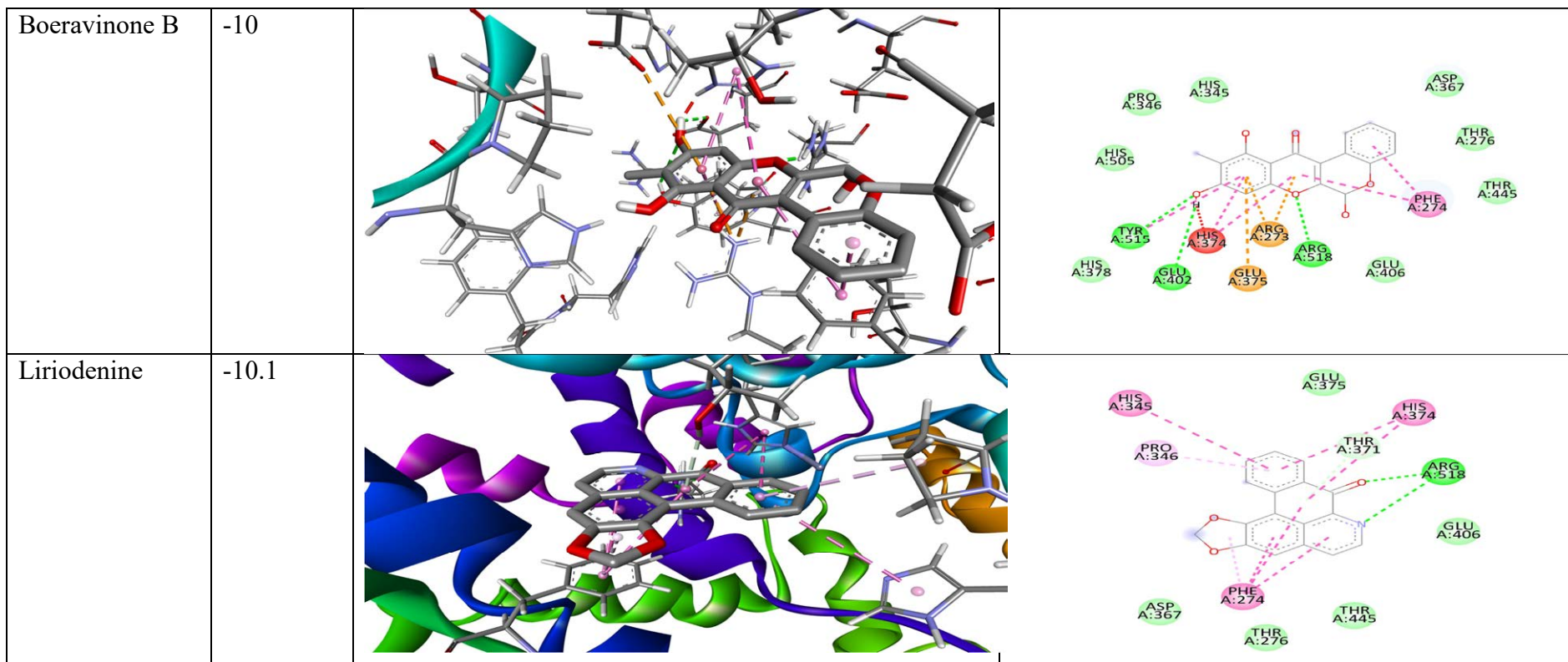
Accepted June 15, 2023

Supplementary data

Table 1. Binding energy, 3D and 2D molecular docking interaction

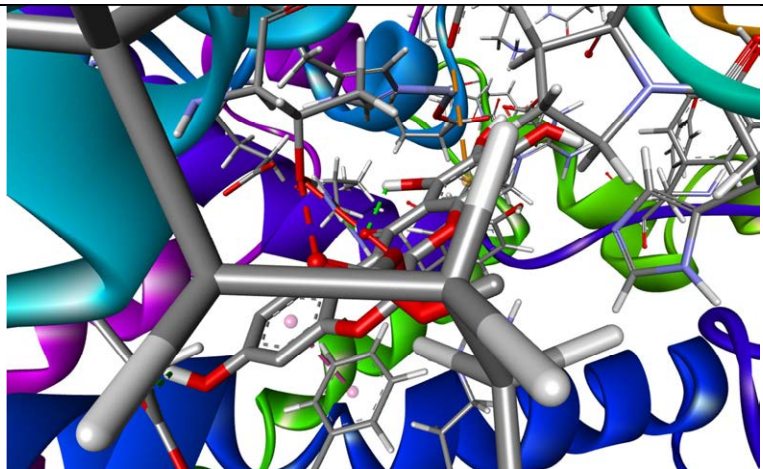
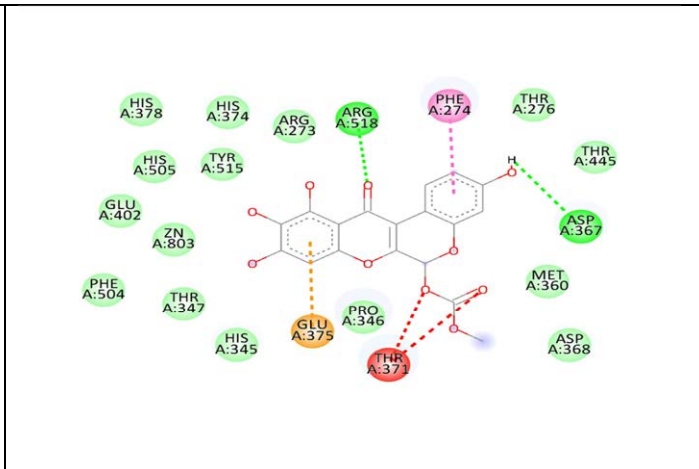
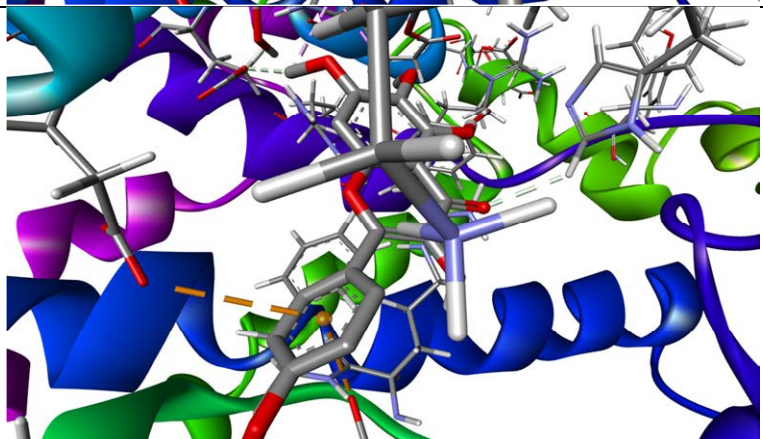
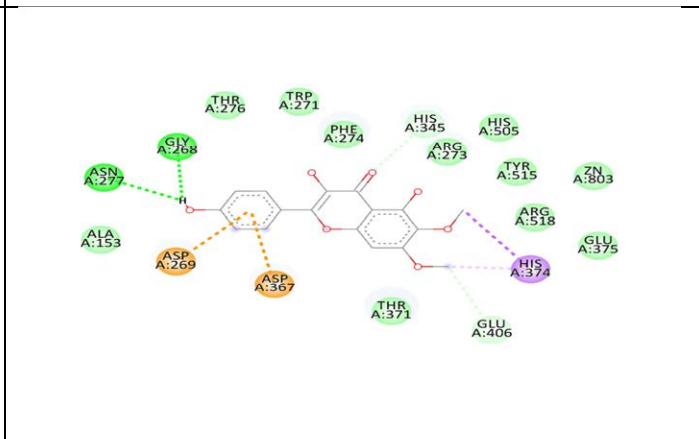
Molecule	Binding energy	3D Docking	2D Docking
L-Arabinose	-5.6		
Boeravinone D	-9.1		
Boeravinone E	-9.5		

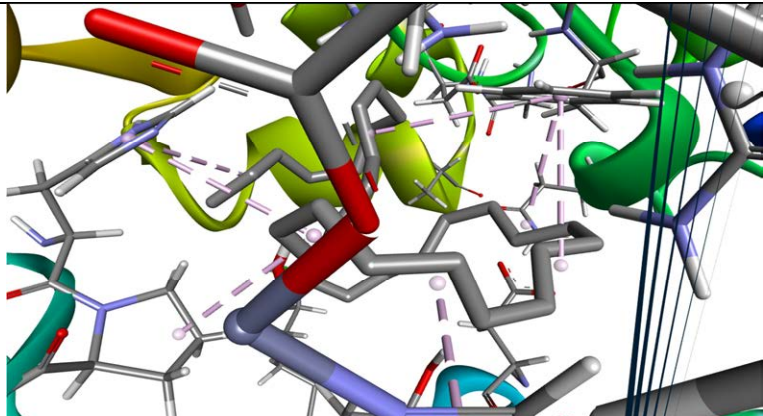
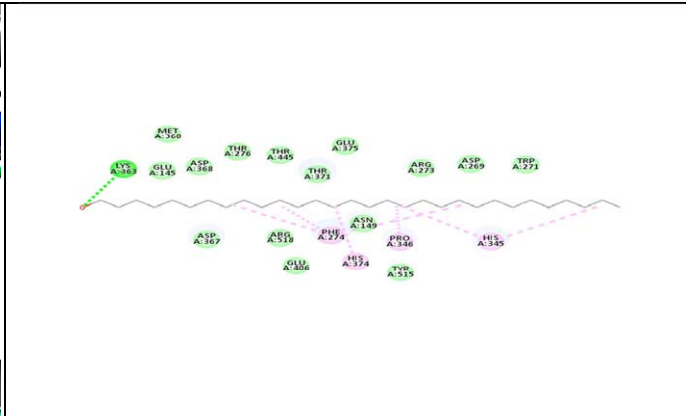
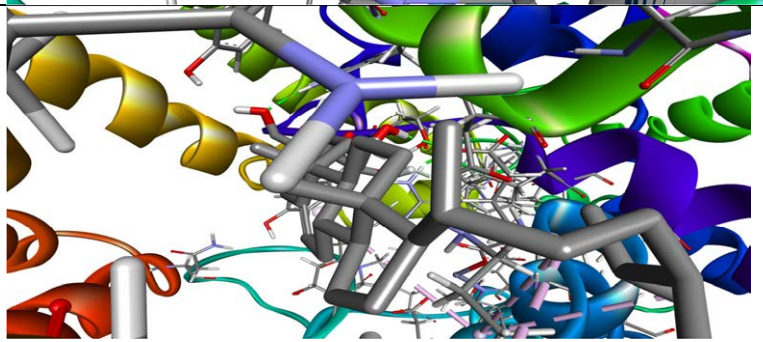
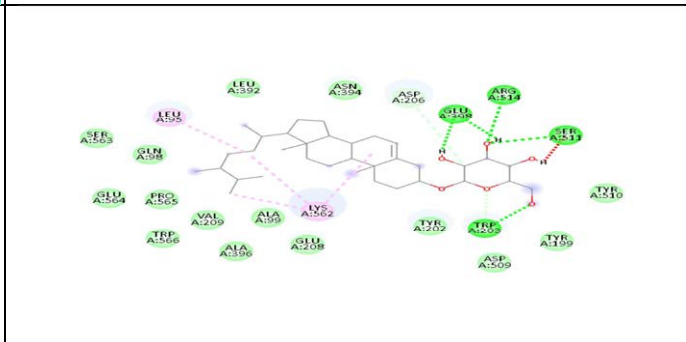
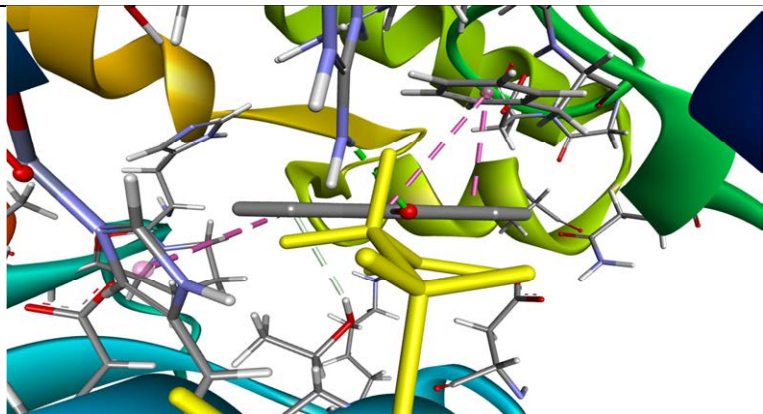
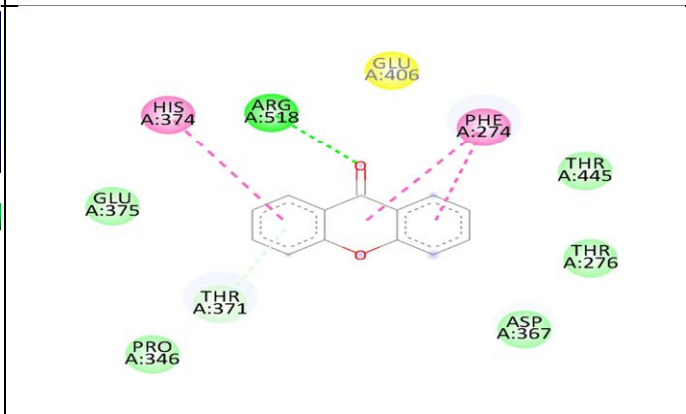




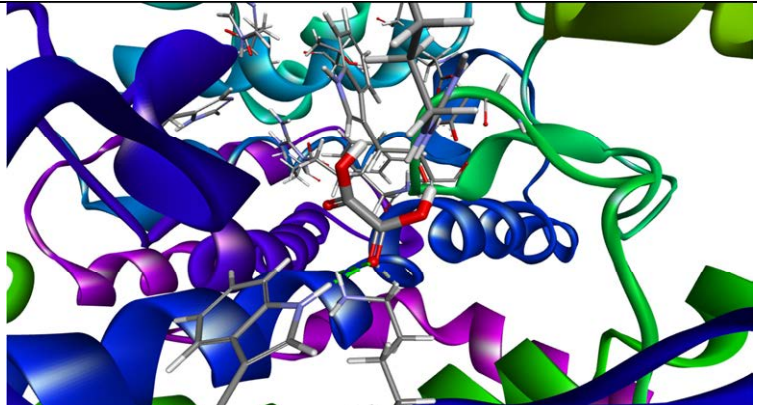
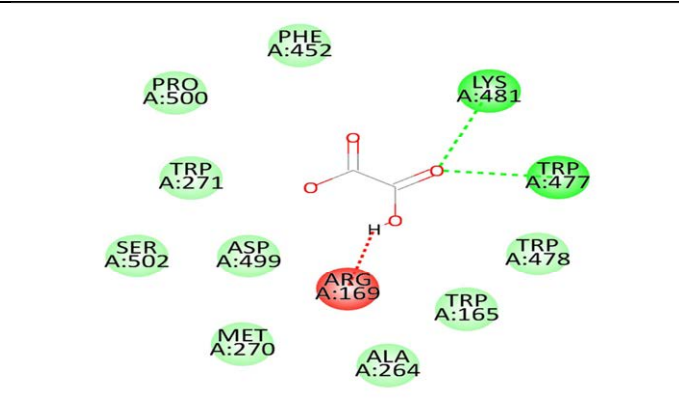
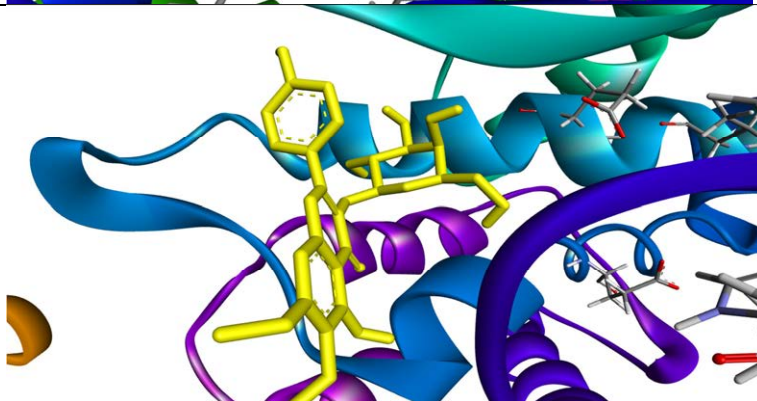
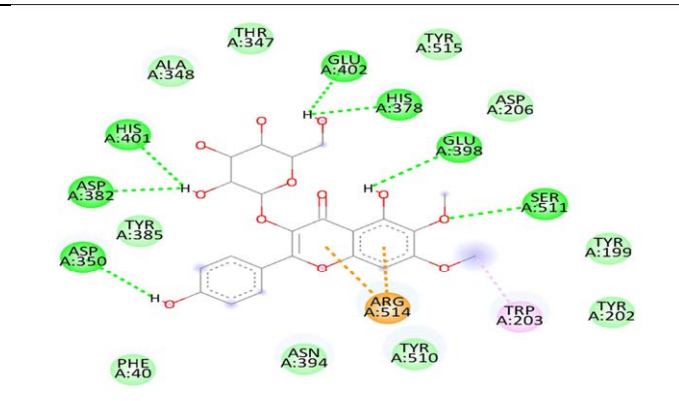
Liriodendrin	-8.5		
D-Glucuronic Acid	-6.4		

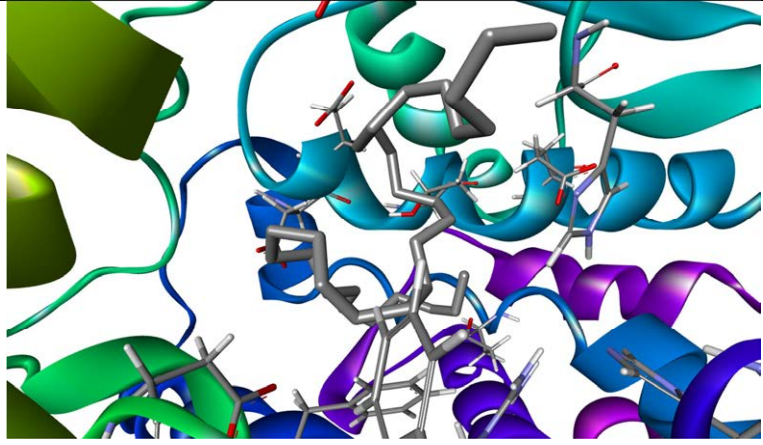
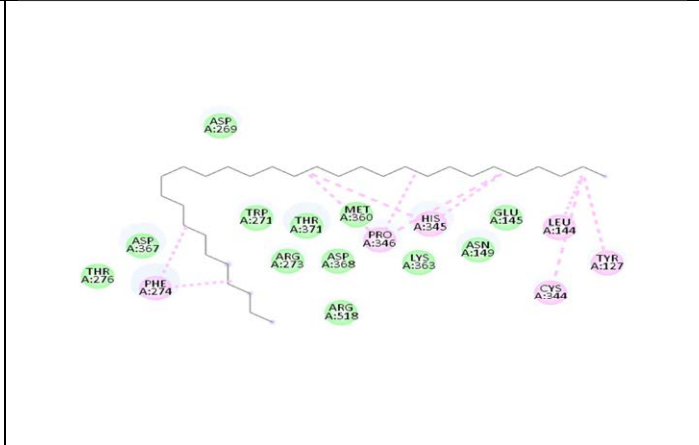
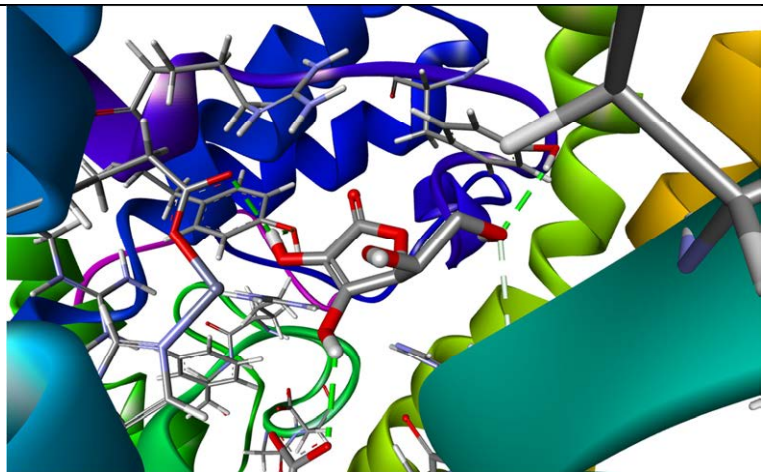
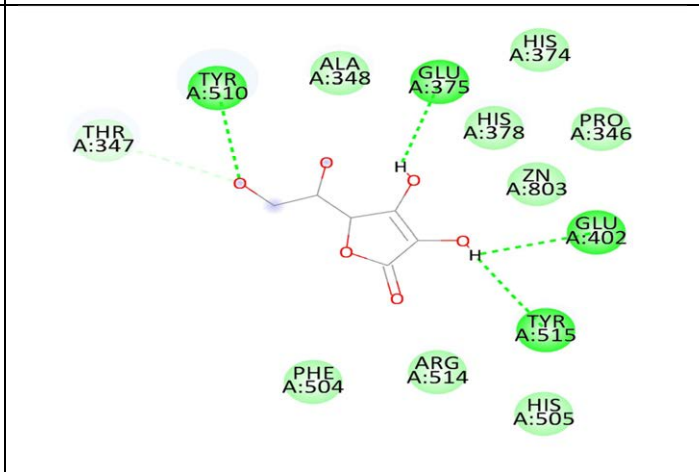
Stearic acid	-5.4		
Repenone	-9.7		

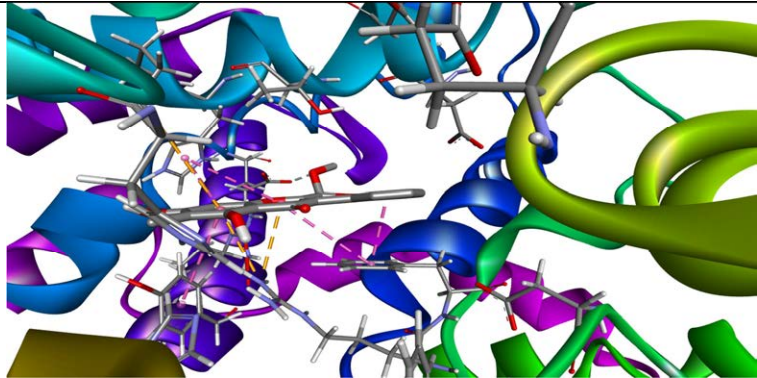
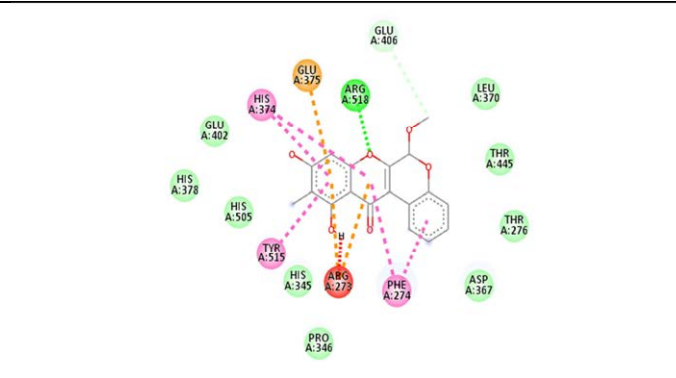
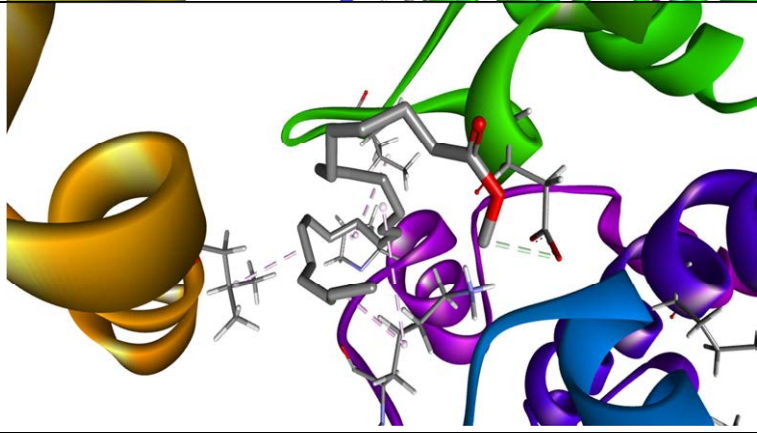
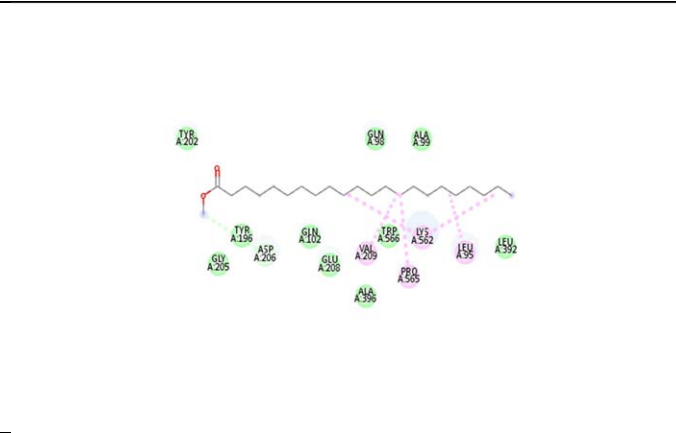
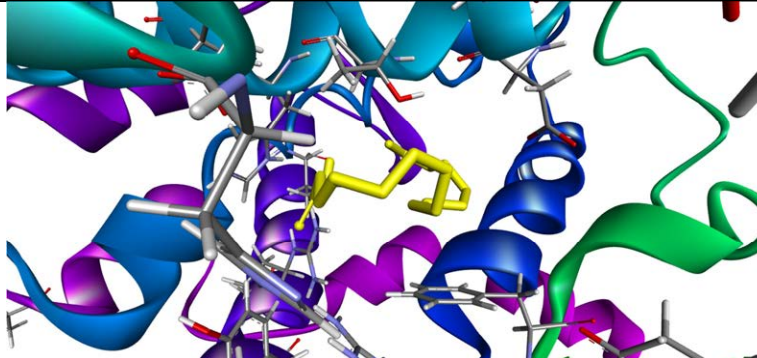
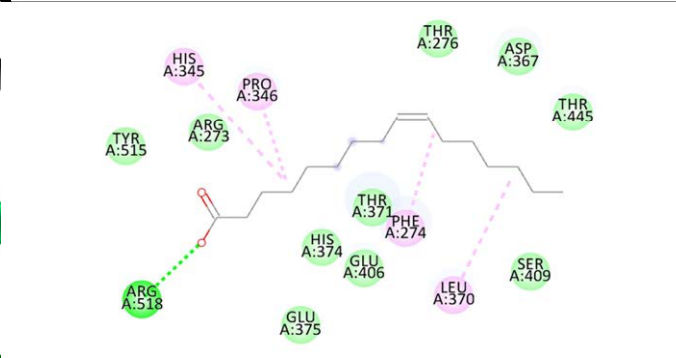
<p>Repenol</p>	<p>-10.3</p>		 <p> HIS A:378 HIS A:374 ARG A:273 ARG A:518 PHE A:274 THR A:276 THR A:445 HIS A:505 TYR A:515 H ASP A:367 GLU A:402 ZN A:803 MET A:360 PHE A:504 THR A:347 PRO A:346 ASP A:368 HIS A:345 GLU A:375 THR A:371 </p>
<p>Eupalitin</p>	<p>-8.4</p>		 <p> THR A:276 TRP A:271 PHE A:274 HIS A:345 HIS A:505 ASN A:277 GLY A:268 TYR A:515 ZN A:803 ALA A:153 ASP A:269 ASP A:367 ARG A:518 HIS A:374 THR A:371 GLU A:375 GLU A:406 </p>

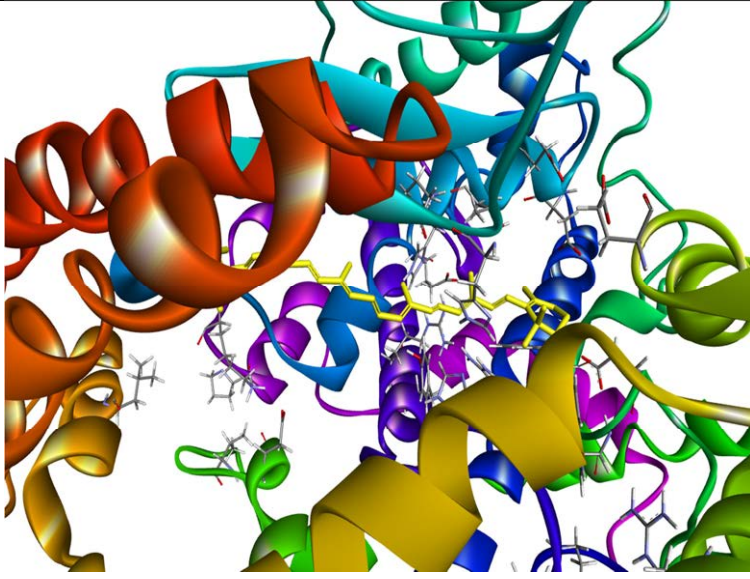
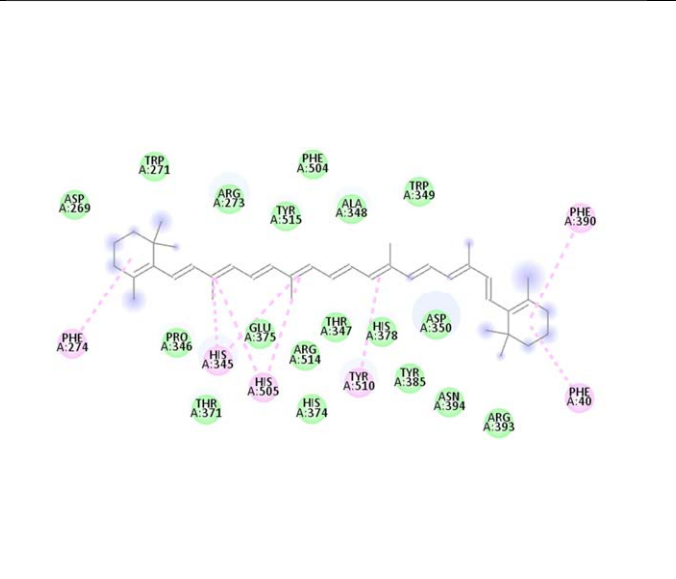
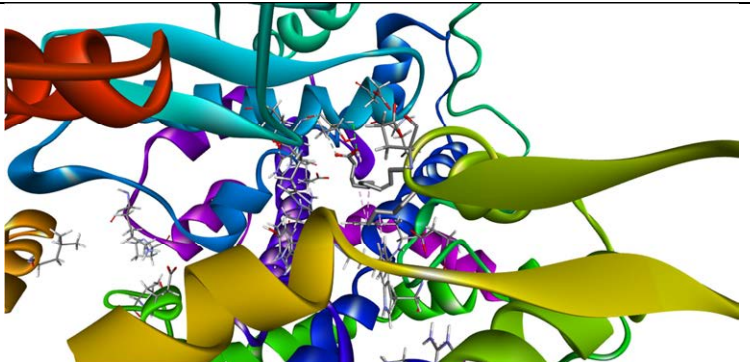
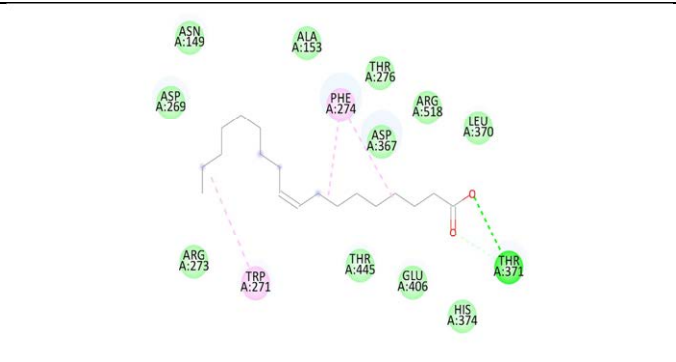
1-Triacotanol	-5.6		
Campesterol glucoside	-10		
Xanthone	-7.7		

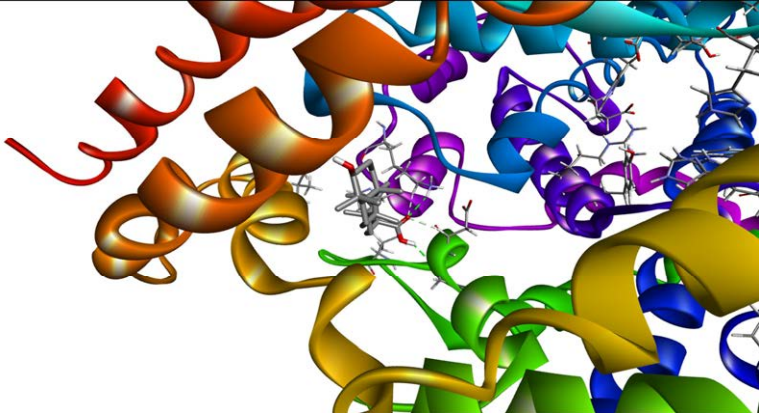
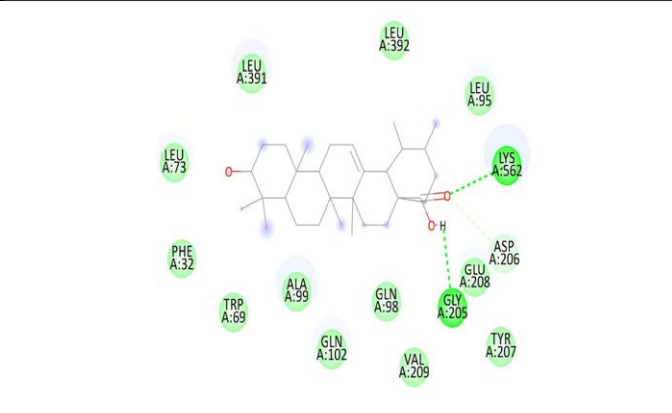
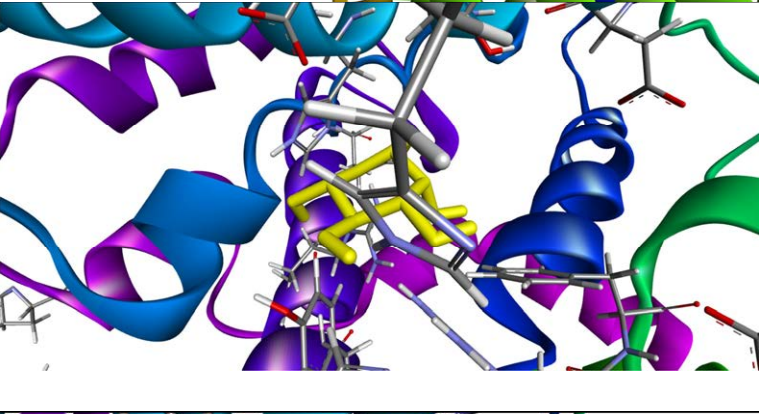
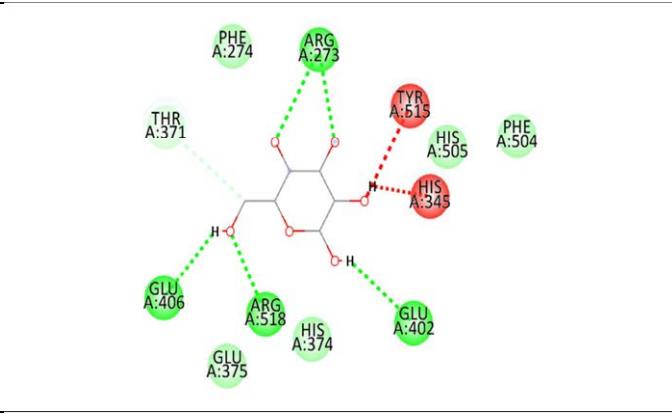
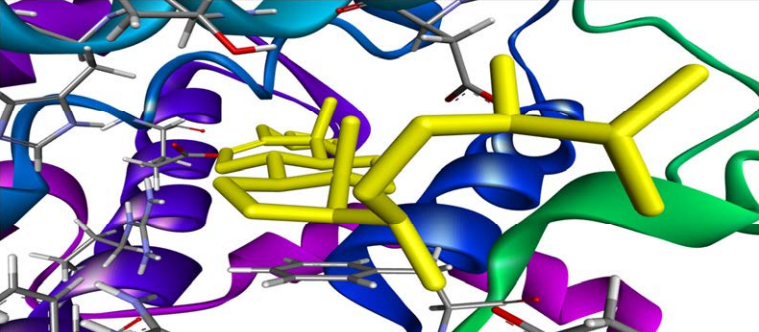
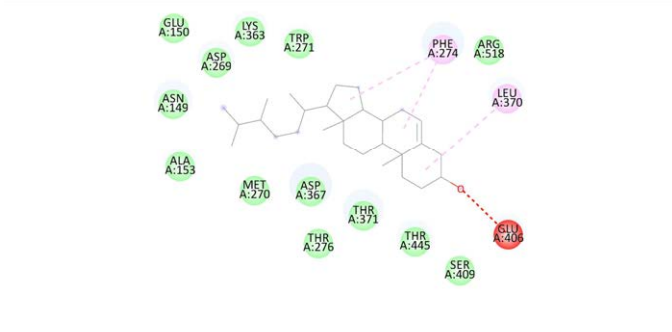
Palmitic Acid	-5.6		<p>Residues interacting with Palmitic Acid:</p> <ul style="list-style-type: none"> TRP A:271 ASP A:269 ARG A:293 PHE A:274 THR A:276 ASP A:367 THR A:445 LEU A:370 ARG A:518 THR A:371 GLU A:406 SER A:409 HIS A:374
Phytic Acid	-7.3		<p>Residues interacting with Phytic Acid:</p> <ul style="list-style-type: none"> ALA A:153 ASN A:277 THR A:276 GLU A:145 ASN A:149 ASP A:269 ASP A:367 MET A:360 ASP A:368 THR A:271 TRP A:271 GLU A:374 THR A:371 PRG A:346 TRP A:145 GLU A:406 ARG A:518 PHE A:274 HIS A:345 HIS A:505 LEU A:503 ARG A:273 GLU A:375 TYR A:515

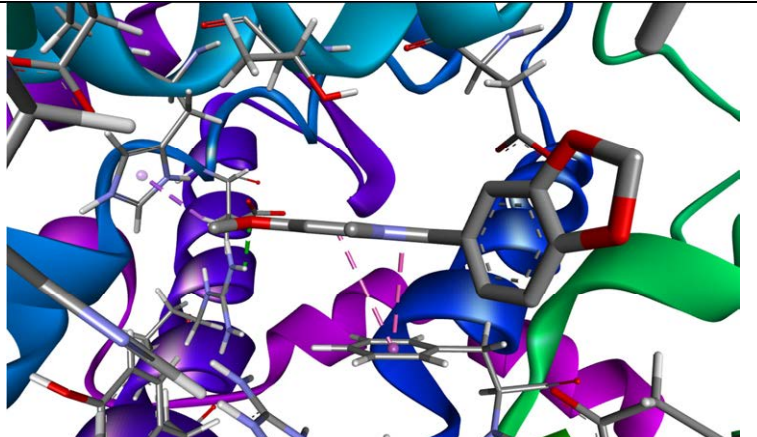
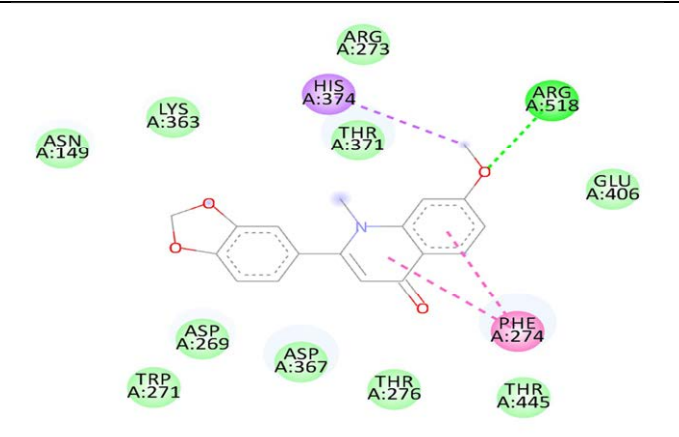
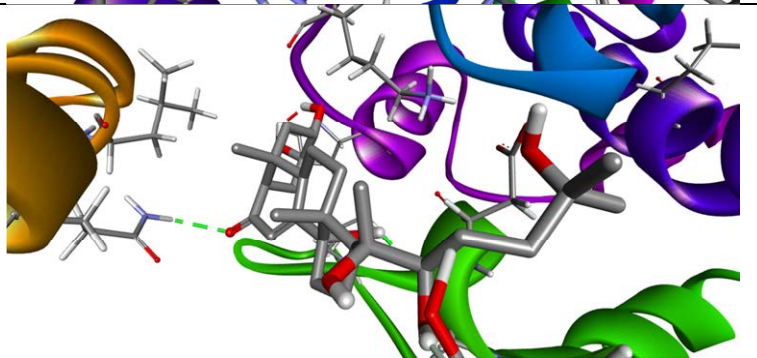
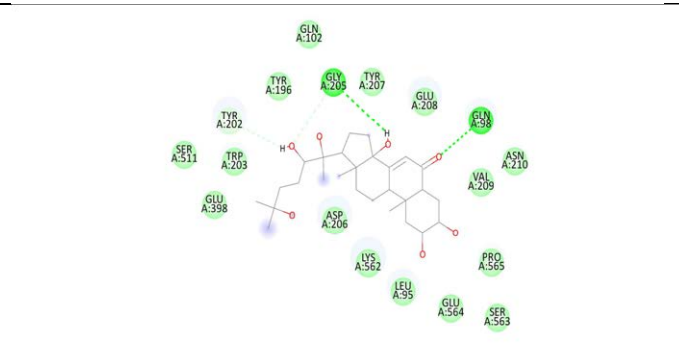
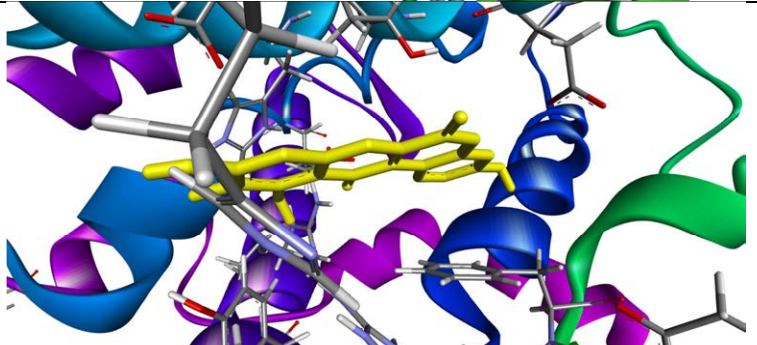
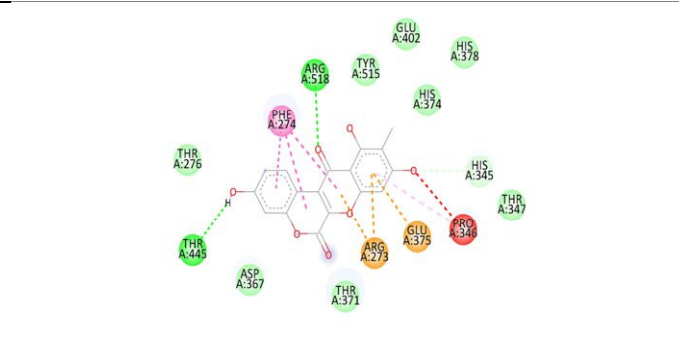
Oxalic acid	-4.4		
Betuletrin	-8.7		

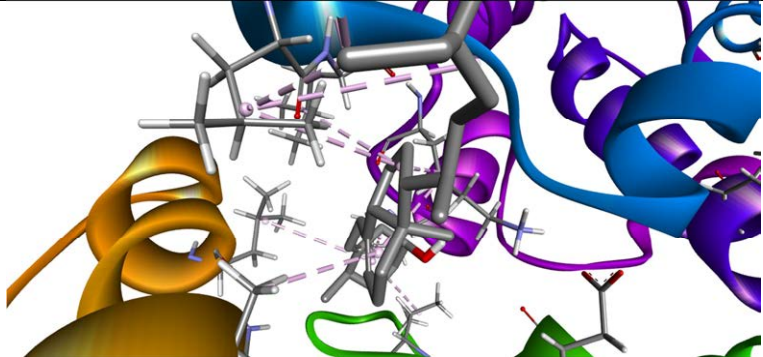
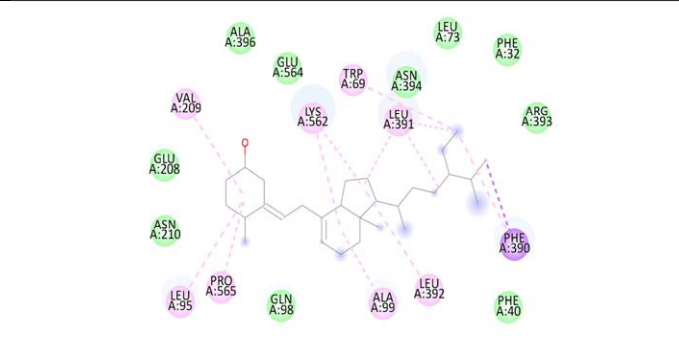
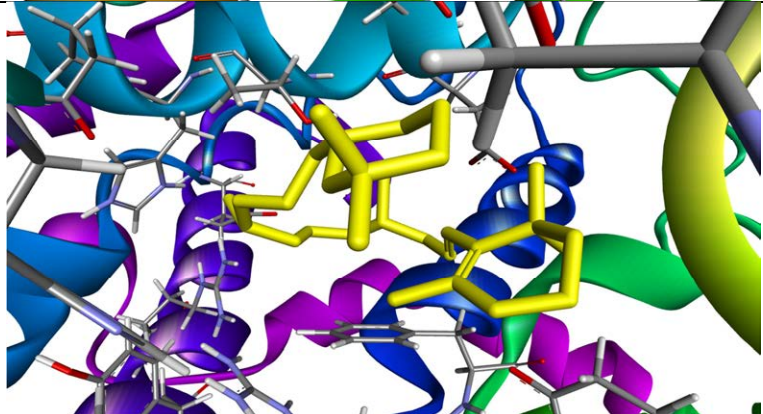
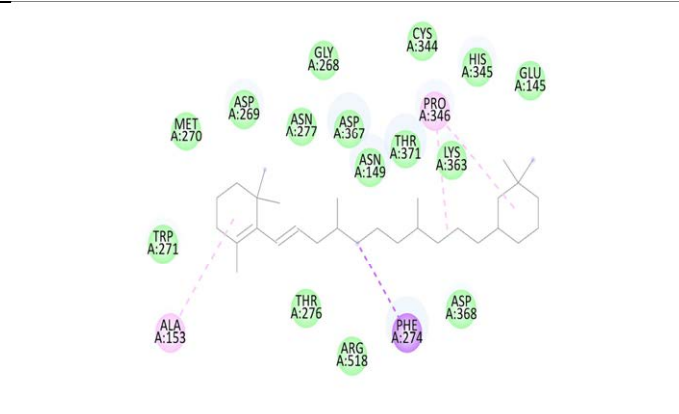
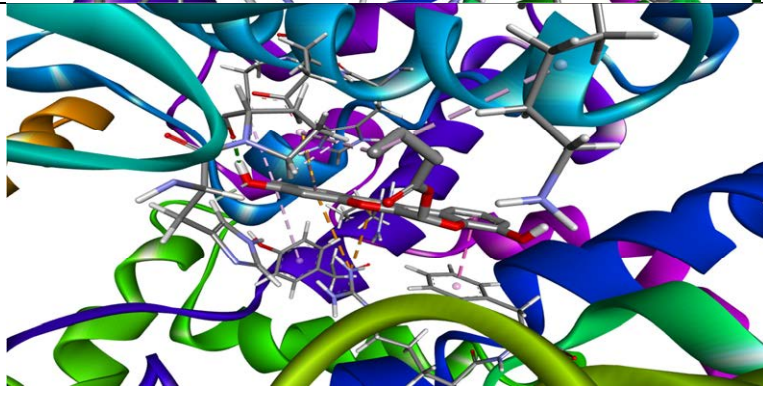
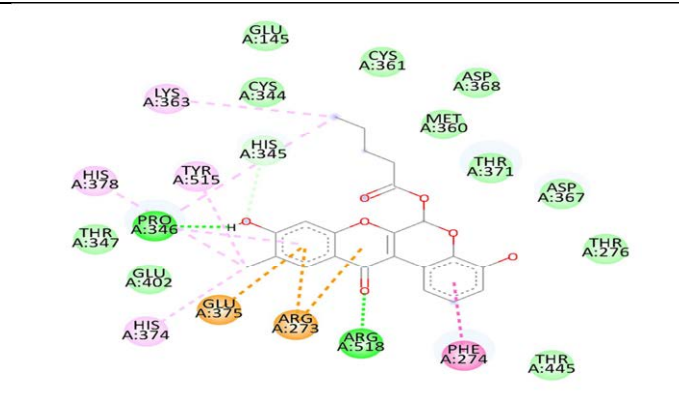
Hentriacontane	-5.8		 <p>Residues interacting with Hentriacontane:</p> <ul style="list-style-type: none"> ASP A:269 TRP A:271 THR A:276 PHE A:274 ARG A:273 ASP A:368 ARG A:318 THR A:371 MET A:360 PRO A:346 LYS A:363 HIS A:345 ASN A:149 GLU A:145 LEU A:144 TYR A:127 CYS A:344
Ascorbic acid	-5.6		 <p>Residues interacting with Ascorbic acid:</p> <ul style="list-style-type: none"> THR A:347 TYR A:510 ALA A:348 GLU A:375 HIS A:374 HIS A:378 PRO A:346 ZN A:803 GLU A:402 TYR A:515 PHE A:504 ARG A:514 HIS A:505

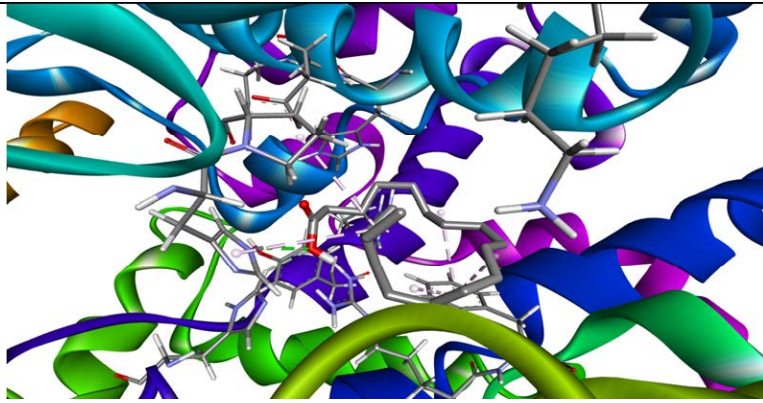
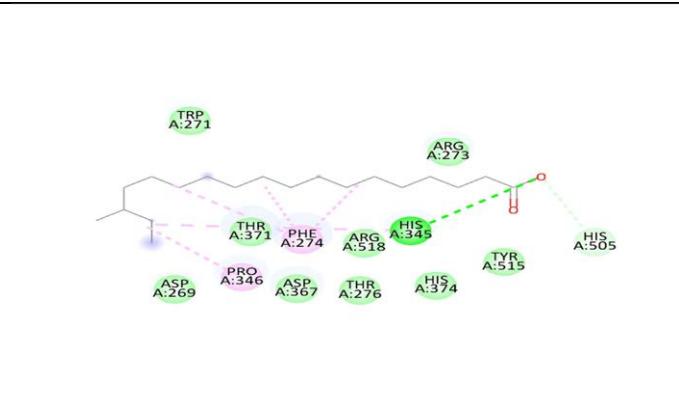
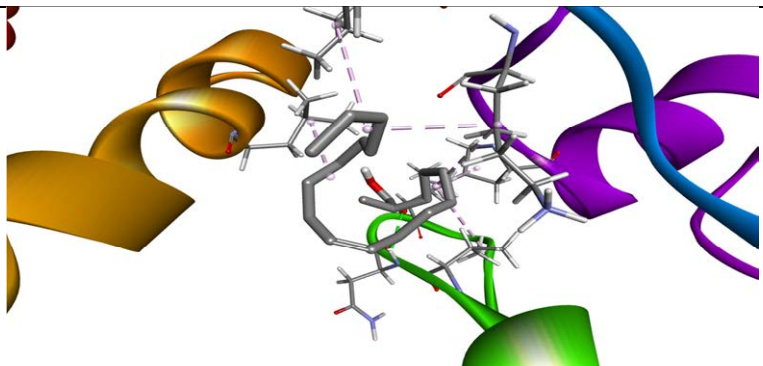
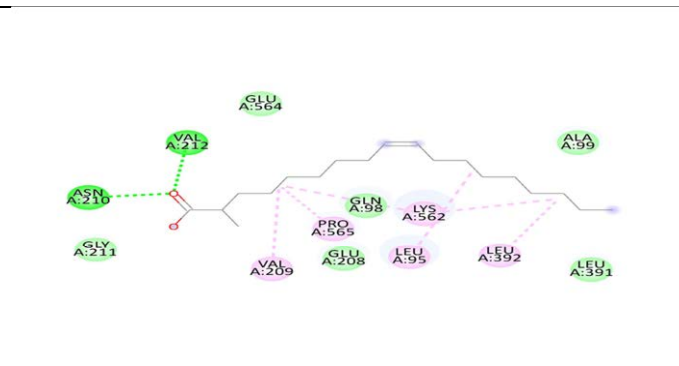
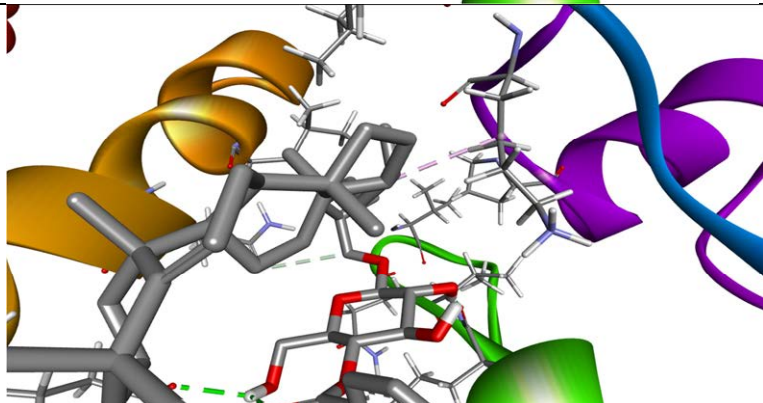
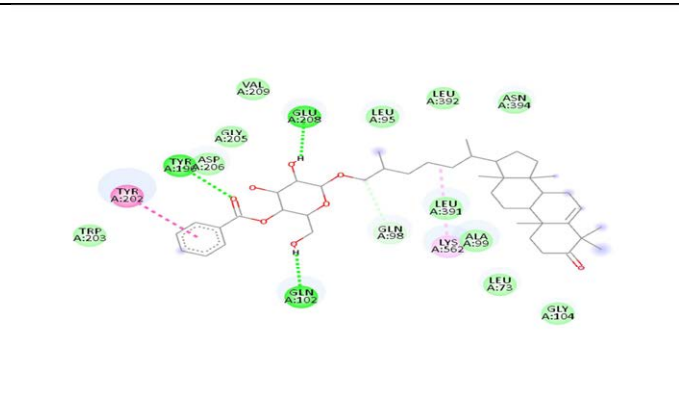
BoeravinoneA	-9.8		
Methyl behanate	-4.7		
Palmitoleic acid	-5.5		

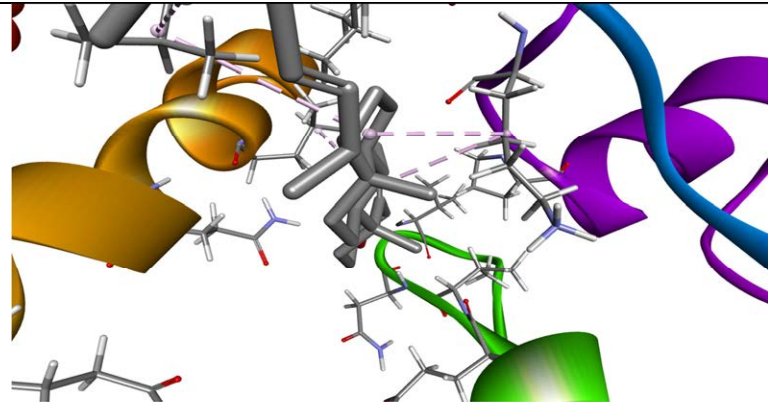
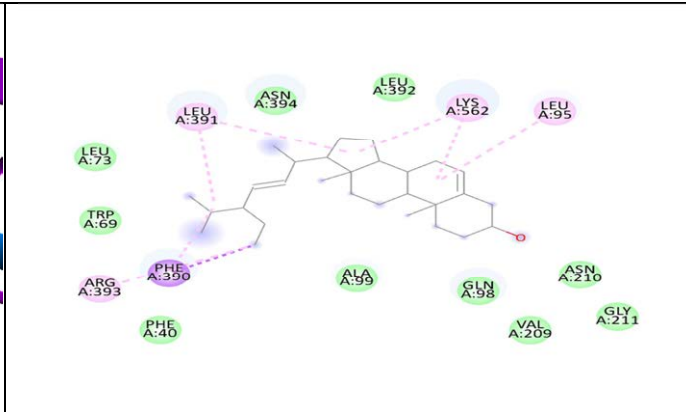
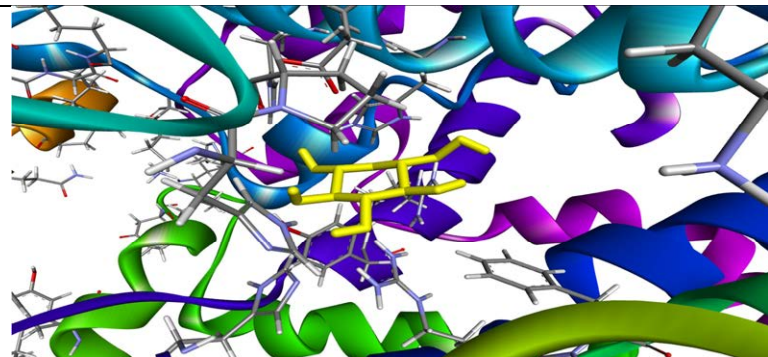
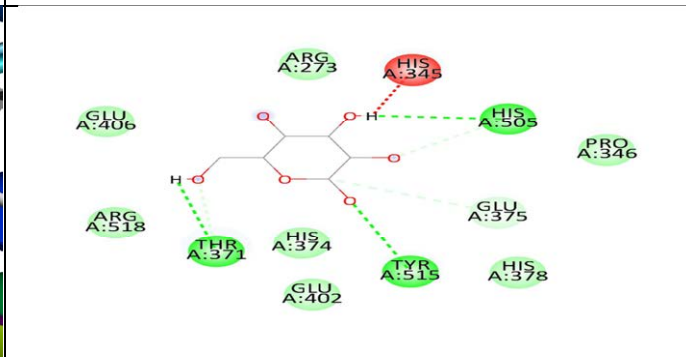
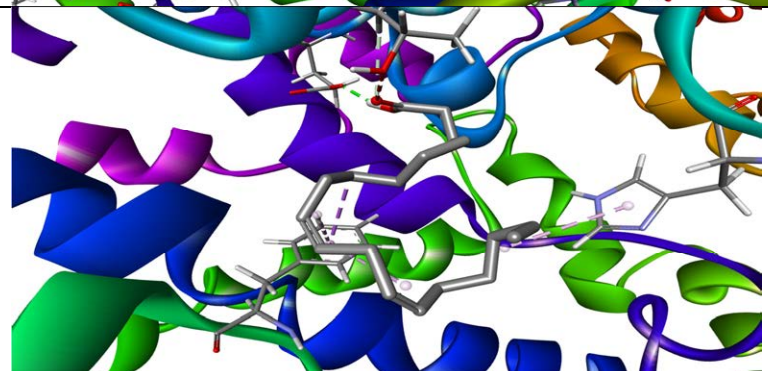
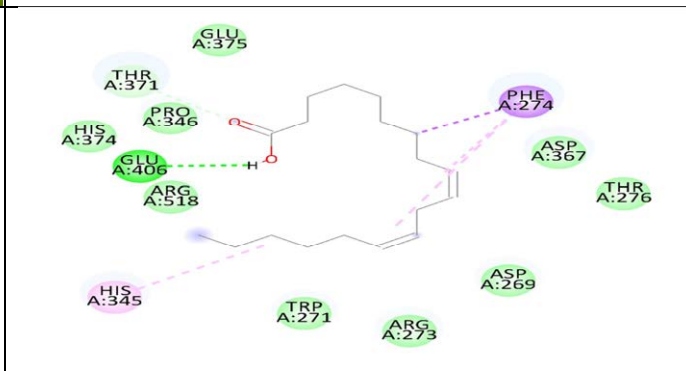
Beta Carotene	-10.7		
Oleic acid	-5.7		

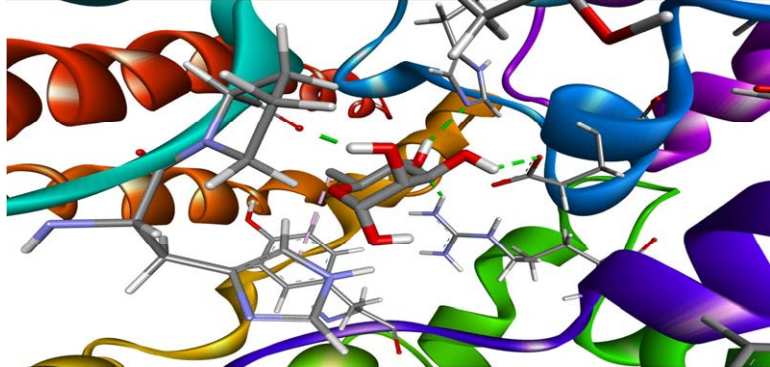
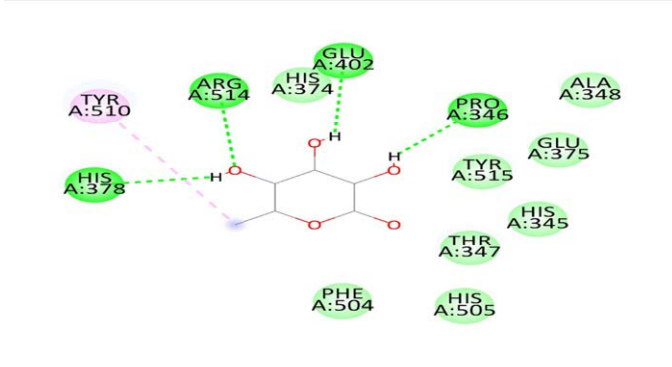
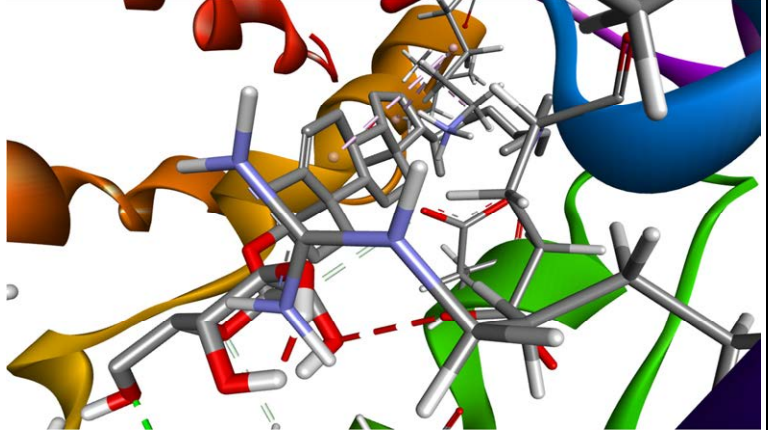
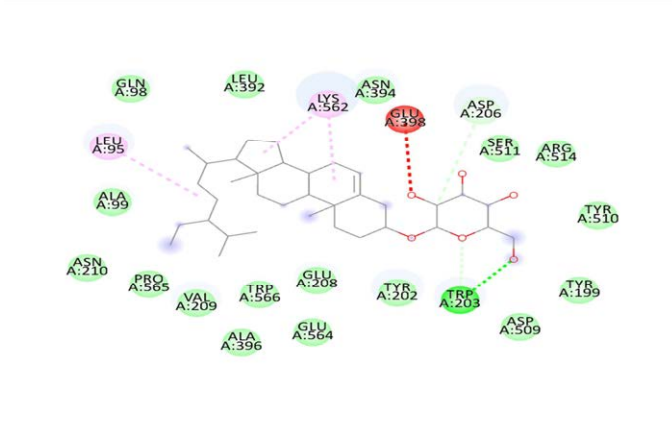
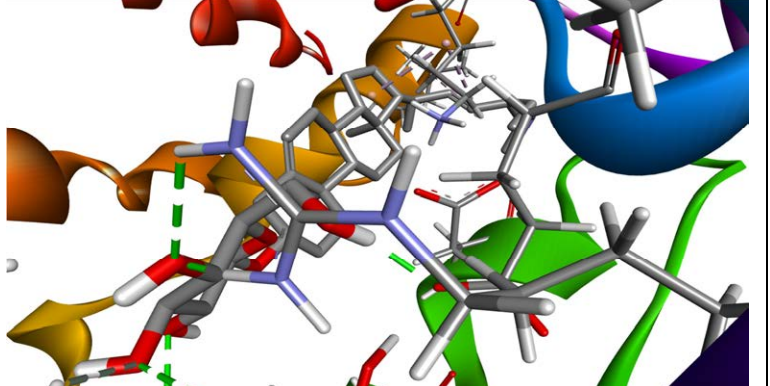
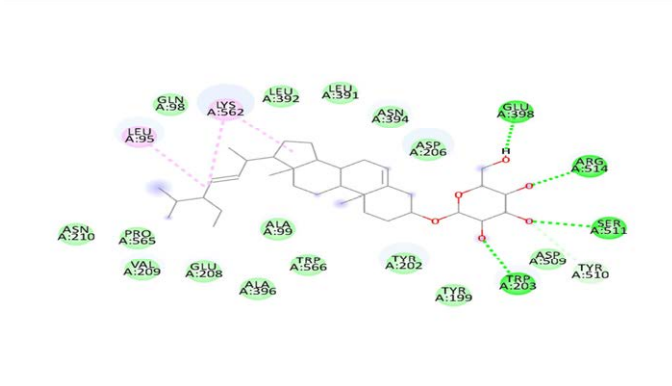
<p>Ursolic acid</p>	<p>-9.5</p>		
<p>D-Galactose</p>	<p>-6.2</p>		
<p>Campesterol</p>	<p>-9.4</p>		

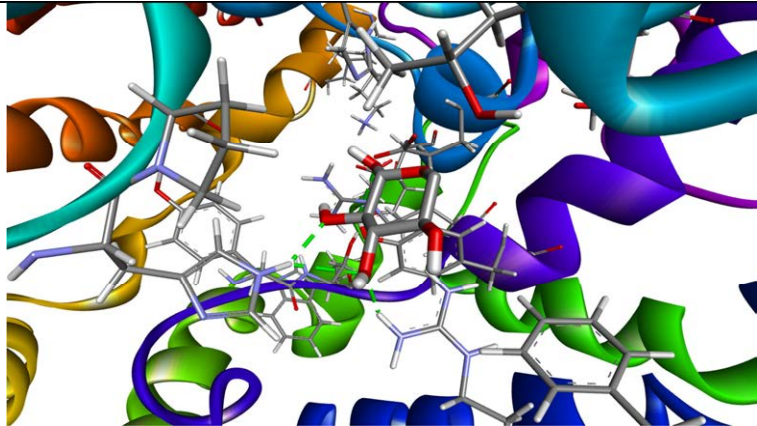
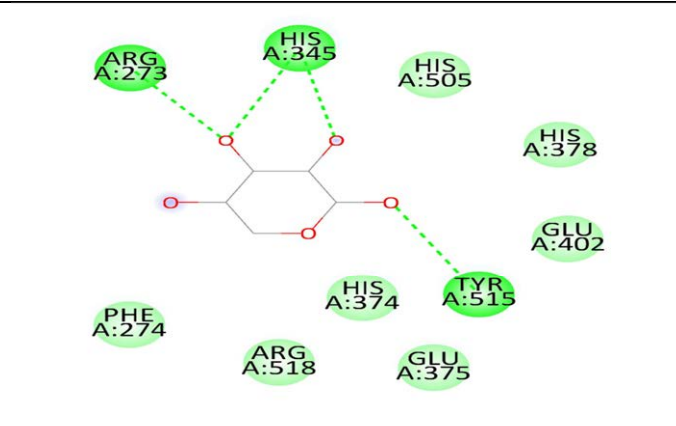
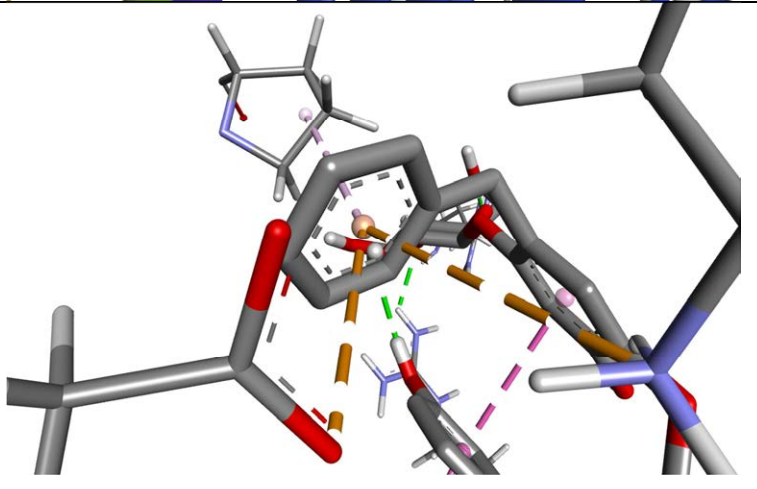
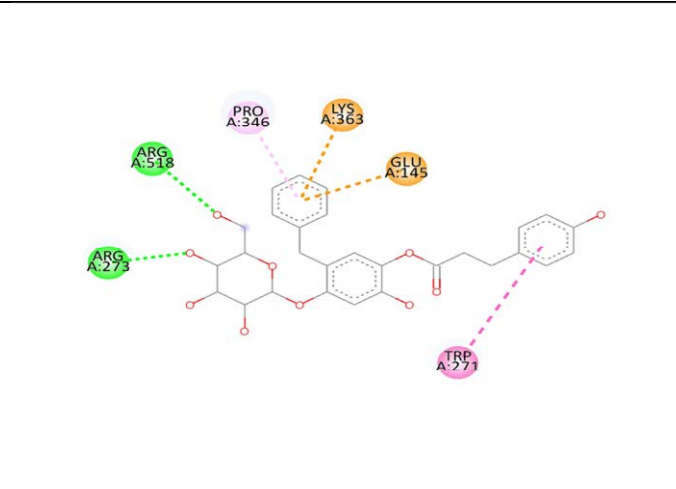
Lunamarine	-9.2		 <p>Residues interacting with Lunamarine: ASN A:149, LYS A:363, ARG A:273, HIS A:374, THR A:371, ARG A:518, GLU A:406, ASP A:269, ASP A:367, PHE A:274, TRP A:271, THR A:276, THR A:445.</p>
20 Hydroxyecdysone	-9.5		 <p>Residues interacting with 20 Hydroxyecdysone: GLN A:102, TYR A:196, GLY A:205, TYR A:207, GLU A:208, LEU A:208, ASN A:210, VAL A:209, SER A:511, TRP A:203, ASP A:206, LYS A:562, LEU A:395, PRO A:565, GLU A:398, LEU A:564, SER A:563.</p>
Boeravinone F	-10		 <p>Residues interacting with Boeravinone F: GLU A:402, HIS A:378, TYR A:515, HIS A:374, HIS A:345, THR A:347, ARG A:518, PHE A:274, THR A:276, THR A:445, ASP A:367, THR A:371, ARG A:273, ARG A:375, PRO A:349.</p>

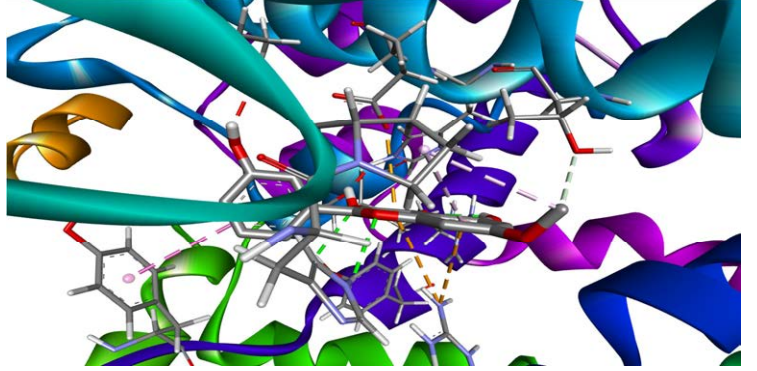
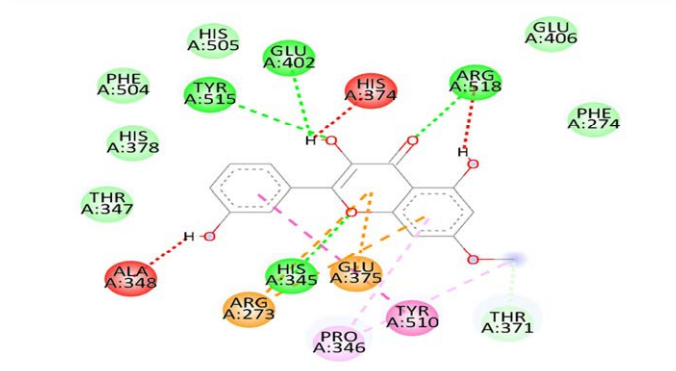
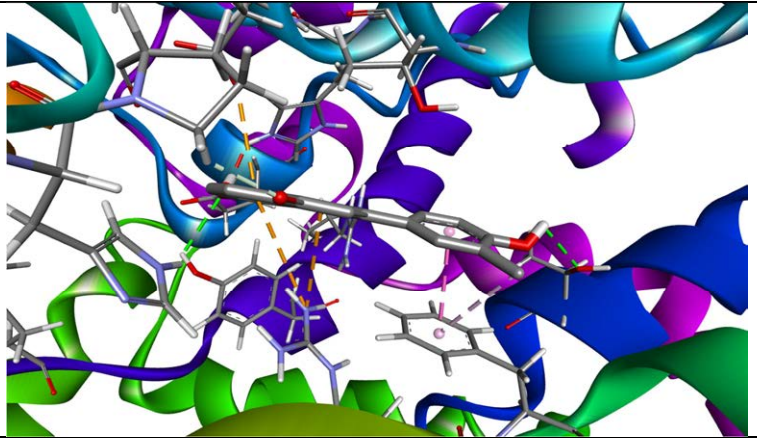
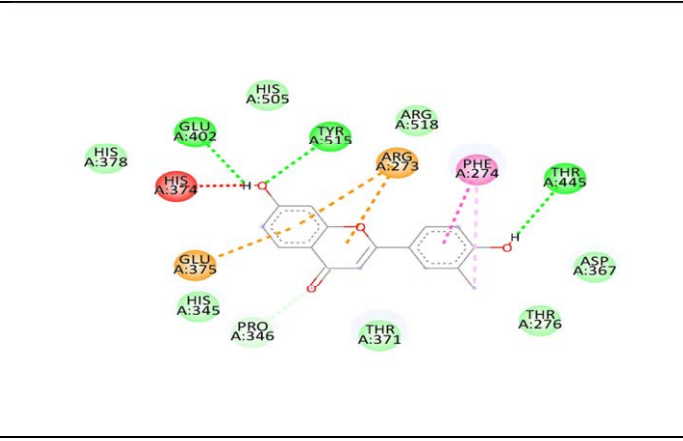
Boerhavisterol	-8.9		
Boerhadiffusene	-8		
Diffusarotenoid	-10.1		

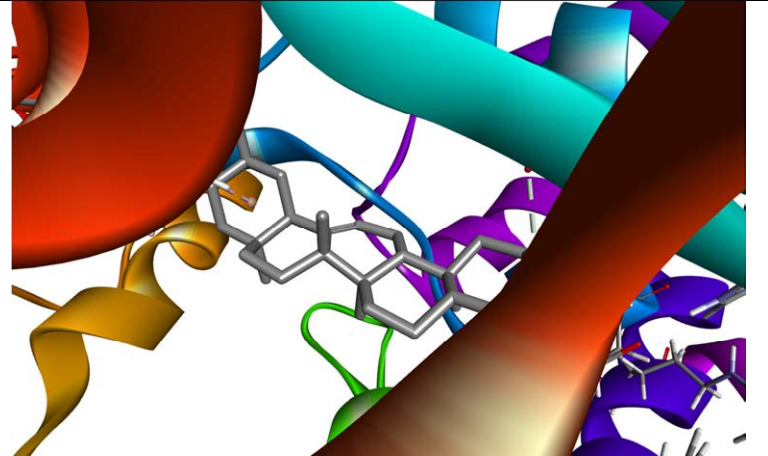
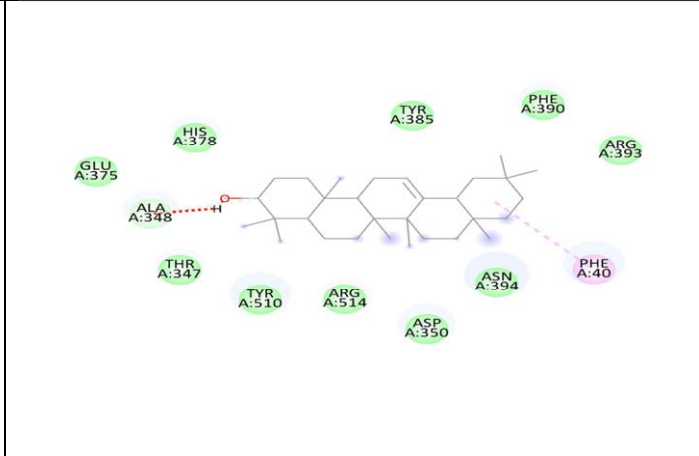
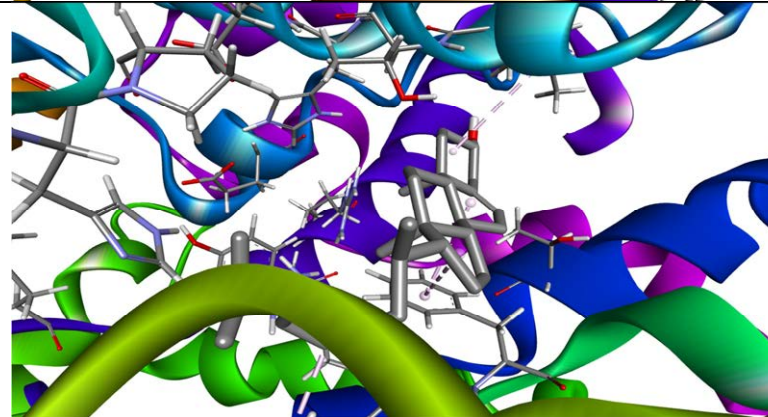
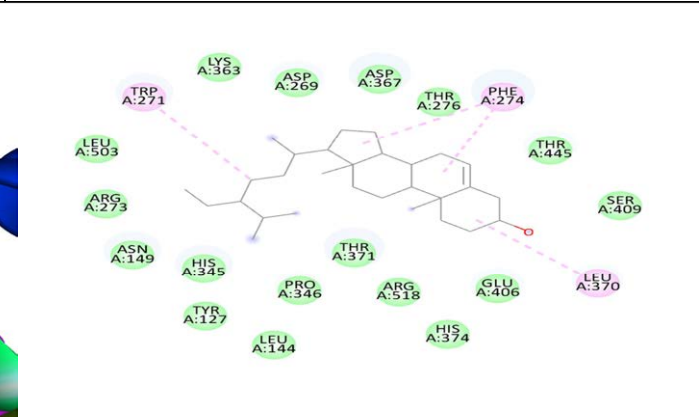
<p>16-Methyloctadecanoic acid</p>	<p>-5.5</p>		
<p>2-Methyl Oleic Acid</p>	<p>-5.4</p>		
<p>Boerhavianostyly benzoate</p>	<p>-9.5</p>		

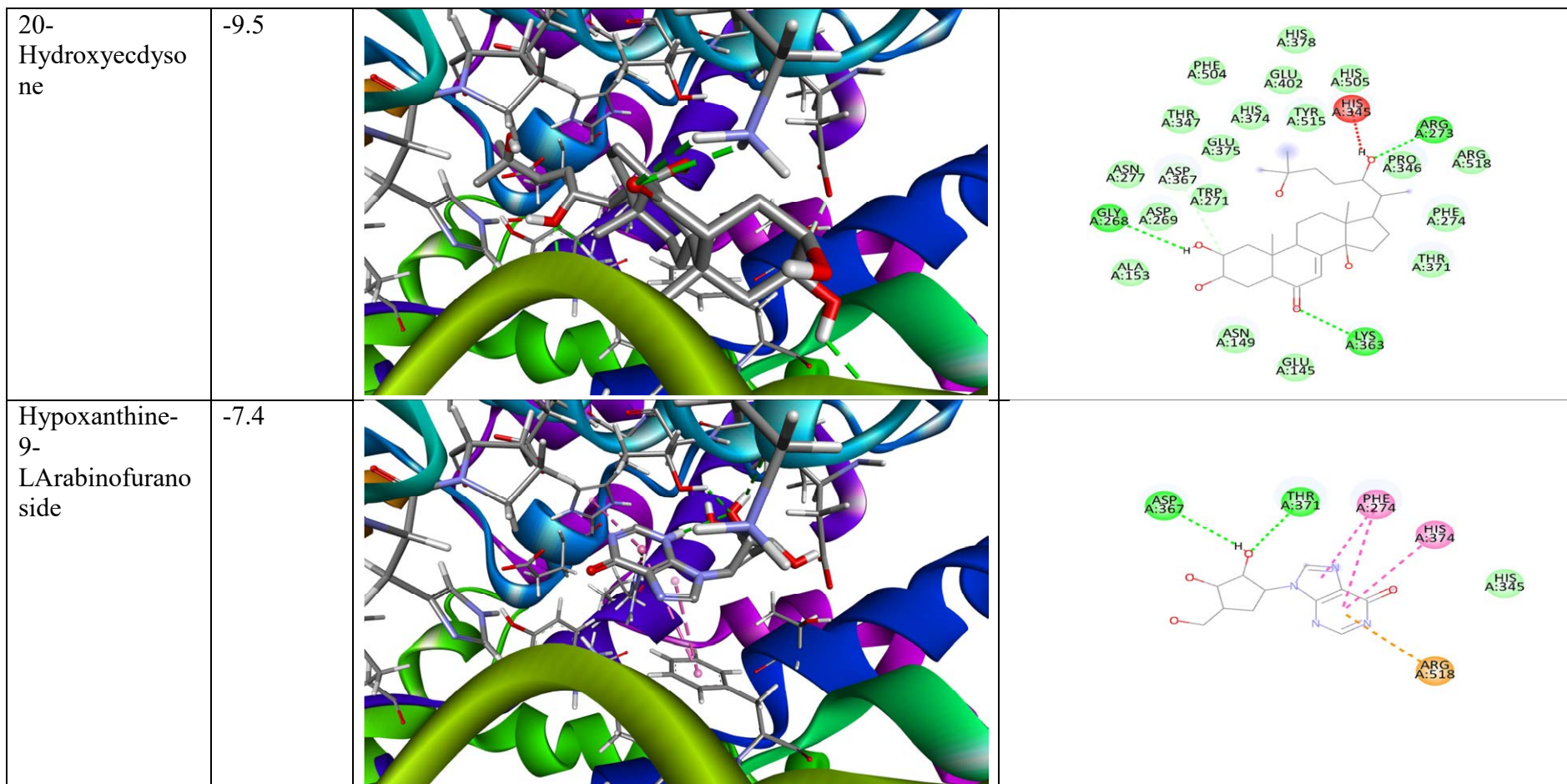
Stigmasterol	-9.3		
D-Glucose	-5.9		
Linoleic Acid	-5.5		

L-Rhamnose	-6		
Stigmast-5-en-3 beta-yl-beta-D-glucopyranoside	-9.8		
Stigmasterol Glucoside	-10		

D-Xylose	-5.3	 <p>A 3D ribbon diagram showing the protein structure in various colors (cyan, orange, purple, green, blue) and the D-xylose molecule in a stick representation. The xylose is bound within a pocket of the protein.</p>	 <p>A 2D interaction diagram showing the D-xylose molecule (a six-membered ring with hydroxyl groups) interacting with several protein residues. The residues are represented by colored circles and connected to the xylose by dashed lines. The residues are: ARG A:273, HIS A:345, HIS A:505, HIS A:378, GLU A:402, PHE A:274, HIS A:374, TYR A:515, ARG A:518, and GLU A:375.</p>
Punarnavoside	-9.5	 <p>A 3D stick model showing the Punarnavoside molecule (a complex polycyclic structure with multiple oxygen atoms) bound to a protein structure. The protein is shown in a grey stick representation, and the Punarnavoside is shown in a stick representation with red and blue atoms. Dashed lines indicate interactions between the molecule and the protein.</p>	 <p>A 2D interaction diagram showing the Punarnavoside molecule interacting with several protein residues. The residues are represented by colored circles and connected to the molecule by dashed lines. The residues are: ARG A:518, PRO A:346, LYS A:363, GLU A:145, ARG A:273, and TRP A:577.</p>

<p>3-3'-5 Hydroxy-7-methoxy flavone</p>	<p>-9.1</p>		 <p>Residues involved in interactions: HIS A:505, GLU A:402, ARG A:518, PHE A:504, TYR A:515, HIS A:374, GLU A:406, HIS A:378, ALA A:348, THR A:347, ARG A:273, HIS A:345, GLU A:375, TYR A:510, THR A:371, PRO A:346, PHE A:274.</p>
<p>4'-7 dihydroxy-3'-methylflavone</p>	<p>-8.9</p>		 <p>Residues involved in interactions: HIS A:505, ARG A:518, THR A:445, HIS A:378, GLU A:402, TYR A:415, PHE A:274, THR A:445, ARG A:273, ASP A:367, GLU A:375, HIS A:345, THR A:371, PRO A:346, THR A:276, HIS A:374.</p>

b-amyrin	-10		
Beta sitosterol	-9.1		



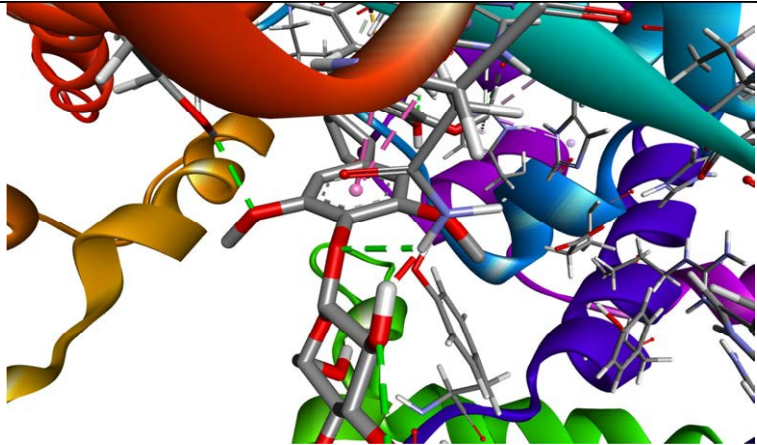
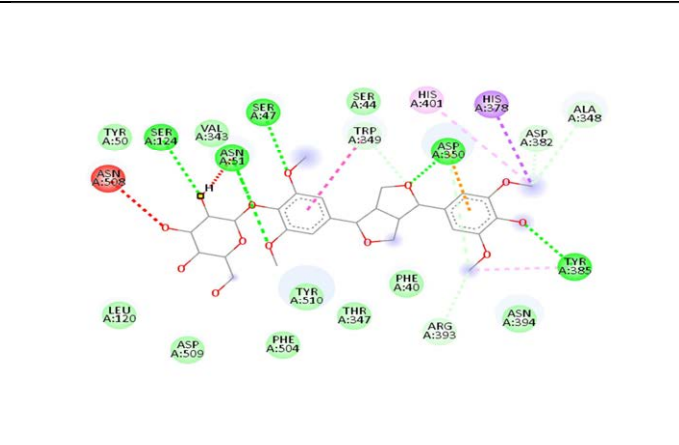
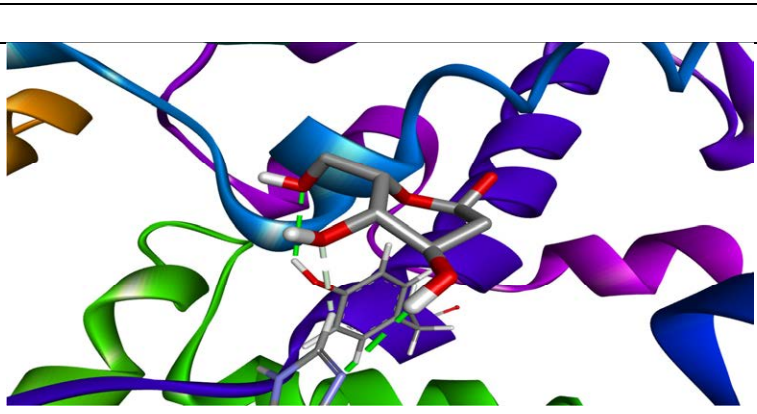
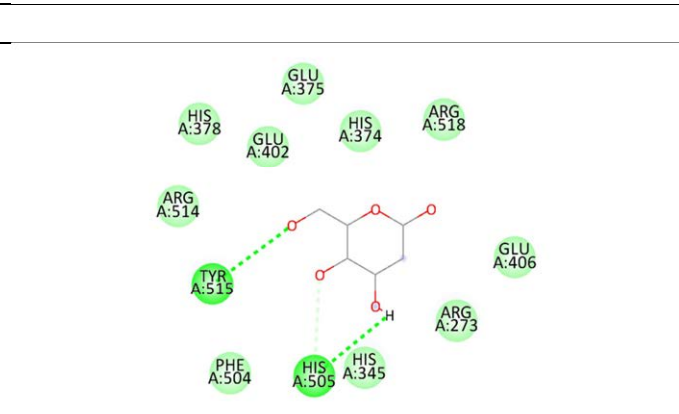
<p>Lignan-Liriodendrin</p>	<p>-8.5</p>		 <p> TYR A:50, SER A:124, VAL A:349, SER A:44, TRP A:349, HIS A:401, HIS A:378, ALA A:348, ASP A:382, TYR A:386, ASN A:394, ARG A:393, PHE A:40, THR A:347, TYR A:510, PHE A:504, ASP A:509, LEU A:120, ASN A:381, ASP A:350 </p>
<p>Standard 2 Deoxy D glucose</p>	<p>-5.7</p>		 <p> HIS A:378, GLU A:402, ARG A:514, TYR A:515, PHE A:504, HIS A:375, HIS A:374, ARG A:518, HIS A:345, ARG A:273, GLU A:406 </p>

Table 2. Binding interaction between ligands and protein 1R4L

Ligand molecule	Binding energy (Kcal/mol)	Amino acid interaction with ligand
Beta carotene	-10.7	Vander waal (18): ASP 269 & 350, TRP 271 & 349, ARG 273, 393, & 514, TYR 515 & 385, ALA 348, PRO 346, THR 371 & 347, GLU 375, PHE 504, HIS 378 & 374, ASN 394. Pi-Alkyl (6): PHE 274, HIS 345 & 505, TYR 510, PHE 390 & 40.
Liriodenine	-10.1	Vander waal (5): ASP 367, THR 276 & 445, GLU 375 & 406 H-bond (1): ARG 518 Pi donar H bond (1): THR 371 Pi-Pi stacked & T-shaped (3): PHE 274, HIS 345 & 374.
Lirodendrin	-8.5	Vander waal (12): GLU 398 & 564, SER 511 & 563, TRP 203 & 199, TYR 510, ASP 509, LYS 187, GLY 205 & 211, ARG 514. H-bond (3): GLN 98, LYS 560, ASP 206. C-H bond (8): PRO 565, LEU 95, VAL 209, LYS 562, GLN 98, GLU 208, TYR 202, ASP 206. Pi-Pi T-shaped (1): TYR 202. Alkyl & Pi-Alkyl (2): LEU 95 & 395. Unfavorable donor-donor (1): ASN 210.
Repenol	-10.3	Vander waal (15): ARG 203, HIS 374, 378 & 505, TYR 515, GLU 402, ZN 803, PHE 504, THR 347, HIS 345, PRO 346, ASP 368, MET 360, THR 276 & 445. H-bond (2): APG 518, ASP 367. Pi-Pi stacked (1): PHE 274. Pi-Anion (1): GLU 375. Unfavorable acceptor-acceptor (1): THR 371.
Diffusarotenoid	-10.1	Vander waal (12): GLU 145, CYS 344 & 361, ASP 368 & 378, MET 360, THR 276, 347, 371 & 445, GLU 402, HIS 345. H-bond: PRO 346, ARG 518. C-H Bond (5): PRO 346, HIS 345, THR 371, ASP 367, PHE 274. Pi-Cation & Anion (2): GLU 375, ARG 273. Alkyl & Pi-Alkyl (4): LYS 363, HIS 374 & 378, TYR 515.
2-Deoxy-D Glucose	-5.7	Vander waal (10): ARG 273, 514 & 518, HIS 345, 374 & 378, GLU 372, 402 & 406, PHE 504. H-bond (2): TYR 515, HIS 505. C-H bond (1): HIS 505.

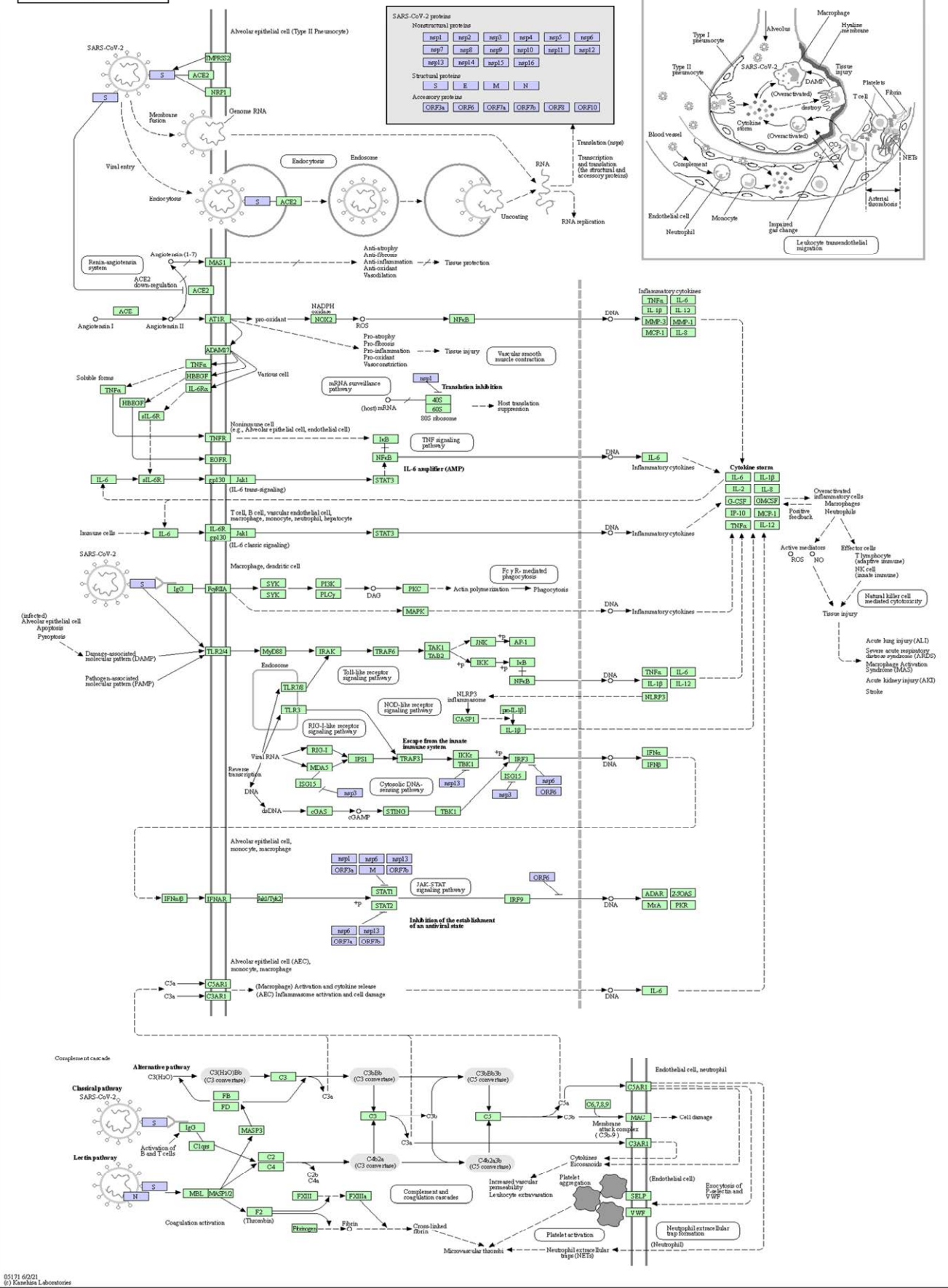


Figure 1. The pathway involved with the ACE2 receptor and coronavirus spike protein substrate